Lattice-Boltzmann Method for Complex Flows

Cyrus K. Aidun and Jonathan R. Clausen

G.W. Woodruff School of Mechanical Engineering, Georgia Institute of Technology, Atlanta, Georgia 30332; email: cyrus.aidun@me.gatech.edu

Annu. Rev. Fluid Mech. 2010. 42:439–72

First published online as a Review in Advance on September 21, 2009

The *Annual Review of Fluid Mechanics* is online at fluid.annualreviews.org

This article's doi:
10.1146/annurev-fluid-121108-145519

0066-4189/10/0115-0439$20.00

Key Words

multiphase flow, microfluidics, turbulence simulation, entropic lattice-Boltzmann, deformable particle suspensions, finite Knudsen number

Abstract

With its roots in kinetic theory and the cellular automaton concept, the lattice-Boltzmann (LB) equation can be used to obtain continuum flow quantities from simple and local update rules based on particle interactions. The simplicity of formulation and its versatility explain the rapid expansion of the LB method to applications in complex and multiscale flows. We review many significant developments over the past decade with specific examples. Some of the most active developments include the entropic LB method and the application of the LB method to turbulent flow, multiphase flow, and deformable particle and fiber suspensions. Hybrid methods based on the combination of the Eulerian lattice with a Lagrangian grid system for the simulation of moving deformable boundaries show promise for more efficient applications to a broader class of problems. We also discuss higher-order boundary conditions and the simulation of microchannel flow with finite Knudsen number. Additionally, the remarkable scalability of the LB method for parallel processing is shown with examples. Teraflop simulations with the LB method are routine, and there is no doubt that this method will be one of the first candidates for petaflop computational fluid dynamics in the near future.

1. INTRODUCTION

Since its introduction two decades ago (Higuera & Jimenez 1989, McNamara & Zanetti 1988), the lattice-Boltzmann (LB) method has been developed into a viable numerical tool for computational fluid dynamics and beyond. With its roots in kinetic theory, the method was developed to build on the strengths and remedy the shortcomings of the lattice-gas automaton (Frisch et al. 1987), while preserving the local nature of the operations and the simplicity of formulation and implementation. The popularity of this method is based in part on its simple formulation and application to flow problems compared with solving the Navier-Stokes (NS) equations, and in part on the high level of scalability on parallel processing systems. In addition to the tremendous progress and advances in the application of this method, fundamental opportunities for further developments exist in various fronts.

We limit this review to the recent developments over the past 10 years as earlier work can be found in the excellent reviews by Benzi et al. (1992) and Chen & Doolen (1998). In particular, we focus on recent developments in LB theory and applications to complex fluid systems, including the suspension of particles and deformable capsules, multiphase flow, microfluidics, entropic LB, and turbulence.

A review of all the publications pertaining to the LB method over the past 10 years would go beyond our space limitations. Therefore, we do not include some important developments that are not within the scope of the immediate topics covered here. Background material on the Maxwell-Boltzmann equation and kinetic theory, as well as other important developments, is available in the **Supplementary Material** (follow the **Supplemental Material link** from the Annual Reviews home page at **http://www.annualreviews.org**). More detailed coverage on the LB method in general is provided in recent books on the general LB method by Succi (2001) and Wolf-Gladrow (2000), an introductory text for geoscientists and engineers by Sukop & Thorne (2006), and applications to shallow-water flows by Zhou (2004).

Supplemental Material

2. THEORY

Several models inspired by the Boltzmann-Maxwell equation have been developed with the motivation of capturing the physics of macroscopic flow through simple local microscale operations. The finite discrete velocity and the LB models are such kinetic-based conservation equations for hypothetical fluid particles, the former with discrete velocities on a spatially continuous domain and the latter with discrete velocities on a discrete regular grid (lattice).

Whereas the applicability of continuum-mechanics-based equations such as the NS and Burnett equations is limited to small or moderate Knudsen number, Kn (the ratio of the molecular mean-free path, λ_m, to flow length scale, H), the Boltzmann equation (BE) can be applied to a wider range of Kn, as discussed in more detail in Section 5.

2.1. Boltzmann-Maxwell Equations

We start our discussion with the conservation equation

$$\left(\frac{\partial}{\partial t} + \mathbf{e}\cdot\nabla_r + \mathbf{a}\cdot\nabla_e\right) f(\mathbf{e}, \mathbf{r}, t) = J, \tag{1}$$

where $f(\mathbf{e}, \mathbf{r}, t)$ is the single particle distribution function, which is defined such that there exists $f(\mathbf{e}, \mathbf{r}, t)\mathbf{dedr}$ particles (by mass) at time t inside the infinitesimal volume element $\mathbf{dr}$ at position $\mathbf{r}$, velocity within the velocity volume element $\mathbf{de}$ with velocity $\mathbf{e}$, and acceleration $\mathbf{a}$. [Normally f has units of (length)$^{-3}$ (velocity)$^{-3}$; in order to not carry m in the relations, we use mf for f

without loss of generality.] We use the shorthand notation of $\mathbf{dr} = dr_1 dr_2 dr_3$ for cubelet integrals over the Cartesian directions. J represents the effect of interparticle collisions and, with Boltzmann's well-known assumptions including the assumption of molecular chaos, gives the BE (see Chapman & Cowling 1970, Huang 1963, Koga 1970). We encourage readers interested in a more detailed review of classical kinetic theory in the context of the LB method to see **Supplemental Appendix A**.

The interest in understanding how fluid dynamics equations can be derived from kinetic theory goes back to the founding works of Maxwell (1867) and Boltzmann (1872). Different asymptotic expansions can be developed for kinetic models to derive various macroscopic hydrodynamic descriptions (Bonilla & Soler 2001). One of the earliest analyses of the BE is by Hilbert (1902, 1912), whose expansion (i.e., the Hilbert expansion) of the dependent variables in terms of Kn results in Euler's equations in the leading order of expansion of the macroscopic variables; however, the NS equations do not appear in Hilbert's solution. Chapman (1916) and Enskog (1917) expanded the distribution function, but not the macroscopic variables, to find Euler's equation in the leading order followed by the NS and the Burnett equations as higher-order expansion terms (Grad 1958). Most commonly associated with the derivation of the fluid dynamics equations from kinetic theory, the Chapman-Enskog expansion, similar to the Hilbert expansion, does not account for the initial- or boundary-value problem. The initial-value (Grad 1963) and boundary-value (Darrozes 1969; Sone 1969a,b) problems are also considered in the limit of small Kn. For a mathematical discussion of the continuum limit of the kinetic equations, we refer the reader to Bouchut et al. (2000).

A discussion of kinetic theory is not complete without mentioning the different timescales and associated dynamical regimes that form the foundation for many of the above analyses. The collision timescale captures the length of particle collisions and can be defined as $\tau_{col} \sim s/e$, where s is a typical particle diameter, and e is the particle velocity. In the BE, this regime is ignored owing to the restriction to two-body interactions that occur instantaneously. The kinetic timescale, $\tau_{kin} \sim \lambda_m/e$, describes the mean time between collisions for a given particle. This scale encompasses the kinetic regime, where relaxation to local equilibrium occurs, but global changes may still persist on larger length scales and timescales. Dynamics in this regime are governed by the BE. The macroscopic timescale governs hydrodynamics and can be described by the convective and diffusive timescales, $\tau_{hyd} \sim L/u$ and L^2/ν, respectively, where ν is the kinematic fluid viscosity.

2.2. Lattice-Boltzmann Method

Before discussing the LB method, we mention the finite discrete velocity model of the BE, where the evolution of hypothetical fluid particles is restricted to velocities that belong to a discrete set $E = \{\mathbf{e}_0, \ldots \mathbf{e}_Q\}$ of Q velocities such that the conservation equation (Equation 1) is given by

$$\partial_t f_i(\mathbf{r}, t) + \mathbf{e}_i \cdot \nabla f_i(\mathbf{r}, t) = J_i(f), \quad i = 0, \ldots, Q, \tag{2}$$

where the discrete one-particle probability distribution function, $f_i(\mathbf{r}, t) \equiv f(\mathbf{r}, t, \mathbf{e}_i)$, specifies the probability of a fluid particle with velocity $\mathbf{e} \in E$ in interval dt at time t inside volume $\mathbf{dr}$ at position $\mathbf{r}$. The transport of the particles is balanced by the particle interactions presented here as the general collision operator $J_i(f)$. The collision operator can be simplified to quasilinear form (Higuera & Jimenez 1989) as

$$J_i(f) = -A_{ij}(f_j - f_j^{eq}), \tag{3}$$

where the distribution function, f_i, has been expanded in terms of Kn into equilibrium f_i^{eq} and nonequilibrium f_i^{ne} components, and A_{ij} is the quasilinear scattering matrix (summation over repeated indices implied). The equilibrium distribution is related to the Maxwell-Boltzmann

equilibrium function (see **Supplemental Equation A.7**). Equation 3 remains nonlinear because of the nonlinear equilibrium distribution function [for a more detailed discussion of the discrete velocity method, including the derivation and properties of the quasilinear collision model and the derivation of the incompressible NS equations in the diffusive limit (Junk & Yong 2003, Junk et al. 2005), see **Supplemental Appendix B**].

We can illustrate the connection between discrete velocity and LB by applying diffusive scaling (Junk et al. 2005) to Equation 2, i.e., $r \to r/\varepsilon$ and $t \to t/\varepsilon^2$, to yield

$$\partial_t f_i(\mathbf{r}, t) + \frac{1}{\varepsilon}\mathbf{e}_i \cdot \nabla f_i(\mathbf{r}, t) = \frac{1}{\varepsilon^2} J_i(f), \quad i = 0, \ldots, Q, \tag{4}$$

where ε is a scaling parameter. Upon integration of Equation 4 along the characteristics, the finite-difference form of the discrete velocity equation can be written as

$$f_i(\mathbf{r} + \mathbf{e}_i\delta_t/\varepsilon, t + \delta_t) - f_i(\mathbf{r}, t) = \frac{1}{\varepsilon^2}\int_0^{\delta_t} J_i(f)(\mathbf{r} + \mathbf{e}_i s/\varepsilon, t + s)\, ds. \tag{5}$$

Approximating the integral over the collision term by the left rectangle rule (note $\delta_t = \varepsilon^2$) results in

$$f_i(\mathbf{r} + \mathbf{e}_i\delta_r, t + \delta t) - f_i(\mathbf{r}, t) \approx J_i(f)(\mathbf{r}, t). \tag{6}$$

By projecting Equation 6 onto a discrete spatial lattice $\{X\}$ invariant under the transformation $\mathbf{e}_i + \{X\} = \{X\}$ and rescaling t and $\mathbf{r}$ such that $\delta_r = \delta_t = 1$, the general LB equation can be written as (McNamara & Zanetti 1988)

$$f_i(\mathbf{r} + \mathbf{e}_i, t + 1) - f_i(\mathbf{r}, t) \approx J_i(f)(\mathbf{x}, t). \tag{7}$$

This is the earliest and most general form of the LB equation, referred to as the nonlinear LB equation. Importantly, the collision operator in Equations 2 and 7 admits multibody collisions, whereas the original BE (Equation 1) is concerned only with two-body collisions with the application limited to short-range interactions in low-density gas flow. Therefore, application to dense fluids (with short-range interactions) becomes possible with the discrete velocity and LB methods. The disadvantage of the nonlinear LB equation is the excessive memory and computational cost associated with the calculation of the collision term; however, for most practical cases, the collision term can be simplified to the quasilinear (Equation 3) or the single-relaxation-time Bhatnagar–Gross–Krook (BGK) collision operator.

The LB equation with a single relaxation time, referred to as LBGK, is given by (Chen et al. 1992, Qian et al. 1992)

$$f_i(\mathbf{r} + \mathbf{e}_i, t + 1) - f_i(\mathbf{r}, t) = -\frac{1}{\tau}(f_i(\mathbf{r}, t) - f_i^{eq}(\mathbf{r}, t)). \tag{8}$$

The relaxation time, τ, and equilibrium function, f_i^{eq}, can be adjusted to recover the incompressible NS equations. The leading four moments of the approximate equilibrium distribution f_i^e with discrete velocity $\mathbf{e}_i$ for incompressible flow (Ma $\ll 1$) are given by

$$\sum_{i=1}^{b} f_i^e = \rho, \tag{9a}$$

$$\sum_{i=1}^{b} f_i^e e_{i\alpha} = \rho u_\alpha, \tag{9b}$$

$$\sum_{i=1}^{b} f_i^e e_{i\alpha} e_{i\beta} = \rho c_s^2 \delta_{\alpha\beta} + \rho u_\alpha u_\beta, \tag{9c}$$

$$\sum_{i=1}^{b} f_i^e e_{i\alpha} e_{i\beta} e_{i\gamma} = \frac{\rho}{3}(u_\alpha\delta_{\beta\gamma} + u_\beta\delta_{\gamma\alpha} + u_\gamma\delta_{\alpha\beta}) + \rho u_\alpha u_\beta u_\gamma, \tag{9d}$$

Table 1 The magnitude and the number of velocity bits for lattice models D3Q15, D3Q19, and D3Q27 and the respective weights, w_i

w_i	No. (2D)	$\lvert\mathbf{e}_i\rvert$	D2Q9	D3Q15	D3Q19	D3Q27
w_0	1	0	4/9	2/9	1/3	8/27
w_1	6 (4)	1	1/9	1/9	1/18	2/27
$w_{\sqrt{2}}$	12 (4)	$\sqrt{2}$	1/36	0	1/36	1/54
$w_{\sqrt{3}}$	8 (0)	$\sqrt{3}$	0	1/72	0	1/216

where Greek indices indicate Cartesian directions. The form of the equilibrium distribution function (see **Supplemental Equation A.8**) for incompressible flow is given by

$$f_i^e(\mathbf{r},t) \approx \rho w_i \left[1 + \frac{(\mathbf{e}_i\cdot\mathbf{u})}{c_s^2} + \frac{(\mathbf{e}_i\cdot\mathbf{u})^2}{2c_s^4} - \frac{u^2}{2c_s^2} + \frac{(\mathbf{e}_i\cdot\mathbf{u})^3}{2c_s^6} - \frac{(\mathbf{e}_i\cdot\mathbf{u})u^2}{2c_s^4}\right] + O(u^4), \qquad (10)$$

where the weighting coefficients, w_i, are determined from the specific discrete velocity sets, given in **Table 1** for the most popular velocity sets, referred to as D2Q9, D3Q15, D3Q19, and D3Q27. In this naming scheme, the first part (DX) refers to the dimensionality, and the second part (QXX) refers to the number of discrete velocity vectors.

By using the LB equilibrium distribution function (Equation 10) and the weight coefficients in **Table 1**, one can verify moments up to $O(u^3)$, where it can be shown that

$$\sum_{i=1}^{b} f_i^{eq} e_{i\alpha}e_{i\beta}e_{i\gamma} - \sum_{i=1}^{b} f_i^{e} e_{i\alpha}e_{i\beta}e_{i\gamma} = \rho u_\alpha u_\beta u_\gamma. \qquad (11)$$

The deviation from a Maxwellian distribution shows loss of Galilean invariance at $O(u^3)$.

The multiple-relaxation-time (MRT) or generalized approach dates back to d'Humières' (1992) pioneering work, which sets up the quasi-linear collision operator A_{ij} in the space spanned by the eigenvectors of the collision matrix. The corresponding eigenvalues represent the inverse of the relaxation time to equilibria. To maintain the stability and separation of physically conserved quantities from nonconserved spurious (ghost) modes, the eigenvalues of the collision matrix are between 0 and 2 (for more detail, see Succi 2001). The development of the MRT model is significant because, in addition to being more stable, it allows one to tune the eigenvalues, expanding the application to a much wider array of fluid and thermal transport systems. In general, the MRT method is more stable than the LBGK method, as demonstrated by d'Humières et al. (2002), and it allows the minimal three-dimensional (3D) model, D3Q13 (d'Humières et al. 2001). Examples of specific applications include important developments in multiphase (Ginzbourg & Adler 1995), free-surface (Ginzburg & Steiner 2002), and thermal (McNamara et al. 1995) flows, viscoelastic models (Giraud et al. 1998), and advective and anisotropic-dispersion equations (Ginzburg 2005).

By expanding the distribution function in Hermite polynomials, assigning a relaxation time to each of the physical moments, and discretizing the velocity space, Shan & Chen (2007) formulate LB models with MRTs. This approach follows the formulation of the LB equation derived from the Galerkin projection of the BGK equation in velocity space (Shan et al. 2006), in which the distribution function is expanded in terms of the Hermite polynomials in velocity space with expansion coefficients in terms of the hydrodynamic moments. Based on this approach, the kinematic viscosity and the thermal diffusivity can be uniquely written in terms of the relaxation times corresponding to the stress tensor and heat-flux moments (see **Supplemental Equations A.4d** and **A.4e**).

With a similar approach to that used for the discrete velocity method, Junk et al. (2005) derive the incompressible NS equation starting from the LB equation

$$f_i(\mathbf{r}+\mathbf{e}_i, t+1) - f_i(\mathbf{r},t) = -A_{ij}[f_j - f_j^{eq}(f)] + g_i(\mathbf{r},t), \qquad (12)$$

with the addition of a force term $g_i(\mathbf{r},t)$. Again, summation convention applies.

Following the same diffusive scaling and asymptotic expansion as in the discrete velocity case, the resulting continuity and NS equations, derived in the same orders, are given by

$$\nabla \cdot \mathbf{u}^{(1)} = 0, \tag{13a}$$

$$\partial_t \mathbf{u}^{(1)} + \mathbf{u}^{(1)} \cdot \nabla \mathbf{u}^{(1)} + \nabla p^{(2)} = \left(\nu^* - \frac{c_s^2}{2}\right) \nabla^2 \mathbf{u}^{(1)} + \mathbf{G}(\mathbf{r}, t), \tag{13b}$$

where ν^* is an eigenvalue of $\boldsymbol{A}$, and $\mathbf{G}(\mathbf{r}, t) = \sum_{i=0}^{Q} \mathbf{e}_i g_i$ is the result of the force term g_i in Equation 12. The viscosity term is now modified because of the constraints from spatial discretization in the LB equation. Upon the substitution of $c_s^2 = 1/3$ and the hydrodynamic eigenvalue of $\boldsymbol{A}$, given by $\tau = \nu^*/c_s^2$ in the viscous term, the familiar LB viscosity coefficient $\nu = (2\tau - 1)/6$ is recovered.

The expansion of the average velocity has the structure $\mathbf{u} = \varepsilon \mathbf{u}^{(1)} + \varepsilon^3 \mathbf{u}^{(3)} + \cdots$ provided the boundary and initial conditions are chosen appropriately (for more details, see **Supplemental Appendix B**). This expansion implies that the solution of Equation 12 recovers terms up to order ε^2 in the NS fields. Considering $\delta_t = \delta_r^2 = \varepsilon^2$, this coupling equates to a first-order accuracy in δ_t and a second-order accuracy in δ_r.

The stability analysis of the LB equation with linear equilibrium distribution shows L^2 stability; that is, the weighted L^2 norm of the solution decreases at each time step for periodic or standard bounce-back boundary conditions (Junk & Yong 2009). Along with the asymptotic analysis outlined above, the stability results can be used to prove the convergence of standard 2D and 3D LB methods to smooth NS solutions for periodic boundary conditions with second-order spatial accuracy for pressure and velocity (Junk & Yang 2009). The same results apply to the case with standard bounce-back for Dirichlet velocity conditions (Junk & Yang 2009).

To improve the stability of the LBGK method while preserving the simplicity and efficiency of the approach, Axner et al. (2007) use a regularized LBGK method based on the scheme proposed by Latt & Chopard (2006). The computed kinetic variables are corrected (regularized) to remove the nonhydrodynamic (ghost) modes. The application to time-periodic Womersley flow shows more accurate and stable results, particularly with the bounce-back method for no-slip boundary conditions (Section 2.4) as compared with the higher-order boundary conditions of Bouzidi et al. (2001) (Section 6.4).

The LB equation must be nondimensionalized to apply to physical problems. The parameters in the LB equation (Equation 8), and hence the governing macroscopic equations, are given in terms of lattice units, i.e., a time step, lattice spacing, and lattice density for the time, length, and density/mass units, respectively. Nondimensionalization is accomplished by introducing the following scales:

$$\left.\begin{array}{ll} \text{Characteristic length scale} & L_s \\ \text{Characteristic velocity} & U_s \\ \text{Reference density} & \rho_s \end{array}\right\}, \tag{14}$$

where these variables are all given in terms of the lattice units discussed above. Following basic dimensional analysis, some nondimensional quantities of interest are

$$\left.\begin{array}{ll} \text{Time} & \hat{t} = \frac{tU_s}{L_s} \\ \text{Length} & \hat{\mathbf{r}} = \frac{\mathbf{r}}{L_s} \\ \text{Density} & \hat{\rho} = \frac{\rho}{\rho_s} \\ \text{Macroscopic velocity} & \hat{\mathbf{u}} = \frac{\mathbf{u}}{U_s} \\ \text{Reynolds number} & \mathrm{Re} = \frac{U_s L_s}{\nu} \end{array}\right\}. \tag{15}$$

This list is not exhaustive, and the characteristic scale λ_m and scaling for microscopic variables (e.g., $\mathbf{e}_i$, c_s) have been omitted for brevity. A direct relationship between lattice and physical

variables is obtained by scaling the physical system by L_p, U_p, and ρ_p and then equating the physical and lattice scaling through the nondimensional variables in Equation 15.

2.3. Entropic Lattice-Boltzmann Method

The shortcoming of the LB approach is the numerical instabilities that arise when the flow velocity or its spatial gradient becomes too large for a given lattice, resulting in negative values of the distribution function. This problem limits the application to relatively small-Reynolds-number flows. The quasilinear LB equation and MRT approaches show improvements over the LBGK but do not remove the instability; additionally, they are more computationally expensive and difficult to implement. Because the H theorem, which enforces positive definiteness in the underlying kinetic equation, is abandoned with the quasilinear and BGK models of the LB method, there are no constraints imposed on the evolution of the distribution functions to ensure their non-negative behavior at every grid point for all times. This problem has long been recognized with various attempts to circumvent it. A promising approach is to introduce a discrete H-theorem constraint that enforces positive definiteness on the distribution functions. These methods, termed entropic lattice Boltzmann (ELB), have led to stable explicit algorithms at small viscosity. A rigorous stability analysis of the ELB method based on detailed balance remains to be done.

Two fundamentally different approaches have been developed, one based on a discretized weighted form of the continuum Boltzmann H function (Ansumali & Karlin 2000, 2002; Ansumali et al. 2003, 2006; Chikatamarla & Karlin 2006; Karlin et al. 1999) and the other (Boghosian et al. 2001, 2003, 2004a,b) based on a Tsallis entropy function (Gell-Mann & Tsallis 2004, Tsallis 1988). The two methods have been reconciled recently (Keating et al. 2007), showing some similarities in the final result. By applying Gauss-Hermite quadratures, one can write the discrete form of the standard continuum Boltzmann H function as

$$H(f_i) = \sum_{i=1}^{Q} f_i \ln\left(\frac{f_i}{w_i}\right), \tag{16}$$

where

$$\sum_{i=1}^{Q} w_i = 1.$$

In the ELB method, the collision term Γ_i is determined so as to extremize H and to remain in balance on a constant entropy surface, that is

$$H(f_1', \ldots, f_Q') = H(f_1, \ldots, f_Q). \tag{17}$$

To ensure that H never decreases, extremization of the functional δH_f with Lagrange multipliers μ (**r**, t) and β_α (**r**, t) given by

$$\delta H_f = \delta \sum_{i=1}^{Q} [b_i(f_i) - \mu f_i - \beta_\alpha f_i e_{i\alpha}] = 0, \tag{18}$$

where $b_i(f_i) = f_i \ln(f_i/w_i)$, subject to the local collision constraints for mass and momentum conservation, results in the exponential form of f_i^{eq}. The Lagrange multipliers are then obtained through the first and second moments ρ and ρu_α. An exact solution for the D3Q27 model is obtained by Karlin and coworkers (1999; Ansumali & Karlin 2000, 2002; Ansumali et al. 2003, 2006; Chikatamarla & Karlin 2006) and is given by

$$f_i^e = \rho w_i \prod_{\alpha=1}^{3} (2 - B)\left(\frac{2u_\alpha + B}{1 - u_\alpha}\right)^{e_{i\alpha}} \quad i = 1, \ldots, 27, \tag{19}$$

where $B = \sqrt{1 + 3u_\alpha^2}$, and weights w_i are given in **Table 1**. The solution for f_i^e in Equation 19 is also valid for velocity models D3Q15 and D3Q19 (Keating et al. 2007). All three velocity models with the exponential f_i^e in Equation 19 satisfy the moments of the Maxwellian up to the fourth order, showing the same $O(u^3)$ error as in Equation 11 (Boghosian et al. 2004b). It seems that decreasing the lattice symmetry by lowering the discrete speeds from D3Q27 to D3Q19 and D3Q15 results in relatively minor distortions, particularly at higher Reynolds numbers (Keating et al. 2007), whereas the reduction of the number of bits leads to lower memory and run-time requirements.

2.4. Boundary Conditions

In this section, we summarize the most widely used no-slip boundary condition for the LB method, the standard bounce-back (SBB). Also, we cover the Lees–Edwards boundary condition (LEbc), which allows the simulation of unbounded shear. A detailed discussion of the LB method as applied to particle suspensions and higher-order boundary conditions is presented in Section 6. Slip phenomena and applications to microfluidics are discussed in more detail in Section 5.

2.4.1. No slip. The most widely used and simplest to implement wall boundary condition is the SBB condition. This method evolved from the boundary conditions of lattice gas and is well documented in the literature (Cornubert et al. 1991, Ginzbourg & Adler 1994, Kandhai et al. 1999, Ladd 1994a, Ziegler 1993). The SBB method resolves the boundary via links crossing the solid boundary from solid to fluid lattice nodes, which are referred to as fluid boundary nodes (FBNs). Fluid distributions propagating along the boundary links are bounced back with an appropriate adjustment of momentum,

$$f_i(\mathbf{r}, t+1) = f_{i'}(\mathbf{r}, t^+) + 2\frac{\rho w_i}{c_s^2}\mathbf{u}_b \cdot \mathbf{e}_i, \tag{20}$$

where t^+ refers to a time postcollision but prepropagation, i' is the direction opposite to i, and $\mathbf{u}_b$ is the local boundary velocity. The transfer of momentum to the solid boundary can be expressed as

$$\mathbf{F}_{i'}^{(b)}(\mathbf{r}_b, t) = -2\mathbf{e}_i\left[f_{i'}(\mathbf{r}, t^+) + \frac{\rho w_i}{c_s^2}\mathbf{u}_b \cdot \mathbf{e}_i\right], \tag{21}$$

where $\mathbf{r}_b$ is the boundary location along the link. When the boundary occurs at the midpoint of these links, the SBB is second-order accurate (Ziegler 1993); however, for more complex boundaries, the accuracy degrades to first order (Ginzbourg & Adler 1994, Noble et al. 1995).

2.4.2. Shear flow in periodic domains. Removing wall effects to determine bulk properties is desirable in many cases (e.g., probing suspension rheology), and simply increasing the domain size of a wall-bounded shear simulation to the extent that wall effects are negligible is computationally prohibitive. Consequently, boundary conditions that are periodic in all directions yet impose shear provide a means to simulate bulk flows in simple shear. Lees & Edwards (1972) developed such a boundary condition for molecular dynamics simulations, termed the LEbc, which is extended to the LB method (Wagner & Pagonabarraga 2002, Wagner & Yeomans 1999). In the LEbc, the flow and vorticity directions are treated in the typical periodic manner; however, in the shear direction, periodic domains are shifted continuously in time with a velocity equal to $\pm\dot{\gamma}H$, where $\dot{\gamma}$ is the imposed shear rate and H is the domain length in the shear direction (**Figure 1*a***). Material crossing the top shear border, both fluid and suspended solids, must undergo a shift in position

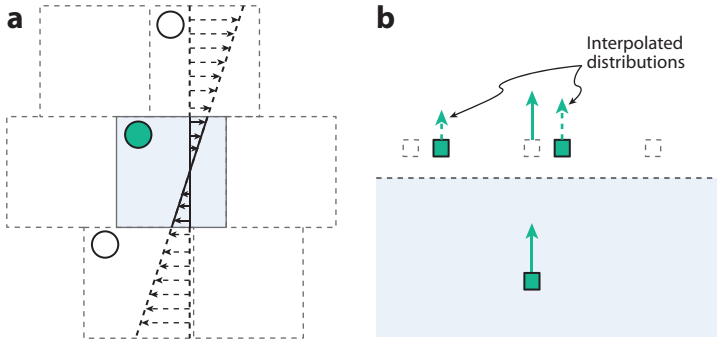

Figure 1

Lees–Edwards boundary condition for the lattice-Boltzmann method. (*a*) A representative particle and periodic domain images (*dotted outlines*) advecting with velocity $\dot{\gamma} H$. The simulation domain is shown as a solid box. (*b*) The required interpolation for distributions propagating from the top to bottom of the simulation domain.

in the flow direction equal to $-\dot{\gamma} Ht$ and a shift in velocity in the flow direction of $-\dot{\gamma} H$ before reappearing in the bottom of the simulation domain.

Implementing the velocity shift in the framework of the LB method requires altering fluid distributions crossing the shear border (**Figure 1*b***). Wagner & Pagonabarraga (2002) propose a Galilean shift to the fluid distributions expressed as

$$f_i^{GS} = f_i + f_i^e(\rho, \mathbf{u} \pm \dot{\gamma} H) - f_i^e(\rho, \mathbf{u}), \tag{22}$$

where f_i^{GS} is the adjusted distribution. Because the positional shift is continuously varying in time, the lattice symmetry is broken, and fluid distributions propagating across the boundary are linearly interpolated to the nearest lattice nodes. The LEbc has been successfully applied to rigid and deformable suspensions in the calculation of shear viscosity with good results (Lishchuk et al. 2006, MacMeccan et al. 2009).

3. TURBULENCE

The potential for direct numerical simulation (DNS) of turbulent flow with the LB method was demonstrated shortly after the LB method's development by comparison with pseudospectral simulations of decaying turbulence (Chen et al. 1992, Martinez et al. 1994) and turbulent shear flow (Benzi & Succi 1990, Eggels 1996, Qian et al. 1995), reproducing the inertial range scaling of $k^{-5/3}$. Sub-grid-scale (SGS) modeling is developed by applying the Smagorinsky (1963) model for the eddy viscosity,

$$\nu_T = (C\Delta)^2 \langle 2 S_{\alpha\beta} S_{\alpha\beta} \rangle^{1/2}, \tag{23}$$

where $S_{\alpha\beta}$ is the resolved strain-rate tensor, the filter width $\Delta = \delta_x$ is the grid scale, and C is the Smagorinsky coefficient. Hou et al. (1996) used this model to modify the relaxation time in the LBGK (Equation 8) by the turbulent relaxation time $\tau = 3(\nu_T(S) + \nu_0) + 1/2$, where ν_0 is the kinematic viscosity, and the total viscosity is given by $\nu = \nu_T + \nu_0$. The interest in applying the LB method to turbulent flow has increased tremendously in both DNS and SGS modeling over the past decade.

The inertial range–consistent SGS modeling (Meyers & Sagaut 2006) used in conjunction with the LB method (Dong & Sagaut 2008) shows promise for more accurate simulation of time-space correlations in turbulent flow. The relation for the Smagorinsky coefficient in the inertial range is

obtained based on the large-eddy simulation (LES) filter width Δ, the Kolmogorov scale, and the ratio of the integral length scale with Δ (Meyers & Sagaut 2006). The modified turbulent eddy viscosity in the inertial range is given by

$$\nu_T^* = \sqrt{(C_\infty \Delta/\gamma)^4 \langle 2 S_{\alpha\beta} S_{\alpha\beta} \rangle + \nu_0^2} - \nu_0, \tag{24}$$

where C_∞ is the Smagorinsky constant based on infinite Re, and γ is a parameter dependent on the shape of the filter. Dong & Sagaut (2008) report a set of simulations for the decay of isotropic turbulence with the LES-LB method using the original (with $C = 0.1$ and 0.18) and modified SGS models with two initial energy spectra: one proposed by Kang et al. (2003) based on their experimental data and one based on the Gaussian spectra. The results are evaluated by comparison with the DNS-LB method and DNS-NS. In all cases, good agreement with the DNS-NS and DNS-LB method is found for single-time statistical quantities. However, the LES-LB method underestimates the time-correlation magnitude for all cases over almost the entire wave-number range. The modified inertial range model performs better than the original SGS model.

An interesting development in the application of the LB method to turbulence is the renewed interest in the analogy between the turbulent fluctuations and microscale thermal fluctuations first suggested by Kelvin (1887). Most notable are the insightful analyses by Chen et al. (2003, 2004), showing the remarkable similarity between the two.

The development of the ELB method holds great promise for high-Re simulations in the transition region, as well as fully turbulent flow. This method, as outlined in Section 2.3, enforces a detailed balance (see **Supplemental Equation A.6**) into the collision operator, where the effective viscosity is adaptively corrected by compliance with the H theorem to have a stable numerical algorithm for arbitrarily high Reynolds numbers (Ansumali et al. 2004, Keating et al. 2007). The ELB method has been used for large-scale turbulence simulation (Vahala et al. 2007) of a 1600^3 grid at sufficiently high Reynolds numbers to find intermittency corrections to the Kolmogorov $k^{-5/3}$ inertial spectrum (Vahala et al. 2009).

Supplemental Material

4. MULTIPHASE FLOW

The four basic LB multiphase methods are the color-fluid model [developed by Gunstensen et al. (1991)], the interparticle-potential model (Shan & Chen 1993, 1994), the free-energy model (Swift et al. 1996), and the mean-field theory model (He et al. 1998). A critical review of each method is provided by Chen & Doolen (1998) and more recently by Nourgaliev et al. (2003). Here, we briefly outline the recent developments of each approach.

The color-fluid model is based on the two-component lattice-gas model proposed by Rothman & Keller (1988), which has been modified by Grunau et al. (1993) to allow variations of density and viscosity. This model is based on red and blue particle distribution functions, $f_i^\alpha(\mathbf{r}, t)$ and $f_i^\beta(\mathbf{r}, t)$, representing two different fluids. The effect of surface tension is obtained through a perturbation step modeled by a collision operator added to the original collision operator, and phase separation is maintained through a segregation step by forcing particles to regions of the same color. Recently, Reis & Phillips (2007) modified the original color-fluid model by adjusting the two-phase flow operator to recover the single-phase NS equations. Lishchuk et al. (2003) used the concept of a continuum surface force to model surface tension directly at the interface. Latva-Kokko & Rothman (2005) proposed a diffusion scheme that solves the lattice pinning problem and creates a symmetric distribution of particles around the interface.

The interparticle-potential model proposed by Shan & Chen (1993, 1994) is based on the concept of nearest-neighbor interaction. To model interactions between the fluid components,

Shan & Chen modified the collision operator by using an equilibrium velocity that includes an interactive force. This force guarantees phase separation and introduces surface-tension effects. This model has been applied with considerable success (Chin et al. 2002; Kang et al. 2002, 2004; Zhang et al. 2001); however, the authors reported some issues with accuracy because the interface is not sharp and the model is not strictly immiscible. To apply the interparticle-potential model to nonideal fluids, Yuan & Schaefer (2006) and Qin (2006) proposed modified interparticle potentials to obtain a suitable equation of state. A multirange interaction model has been proposed (Falcucci et al. 2007, Sbragaglia et al. 2007) and quantitatively studied by Chibbaro et al. (2008) to control the surface tension independently of the equation of state.

The free-energy model proposed by Orlandini et al. (1995) and Swift et al. (1996) uses a free-energy function to include surface-tension effects in a thermodynamically consistent manner. Contrary to the two previous models, this model considers the total density ρ and the density difference $\Delta\rho$ as simulation parameters instead of the density of each phase. The two distribution functions that describe the evolution of ρ and $\Delta\rho$ are governed by the LBGK equation. The lack of Galilean invariance is the primary shortcoming of the original free-energy model and has been investigated, notably by Holdych et al. (1998), Inamuro et al. (2000), and Kalarakis et al. (2002). Zheng et al. (2006) and Inamuro et al. (2004) proposed two new free-energy models that can simulate multiphase flows with high density ratios (up to 1000). Zheng et al. use the convective Cahn-Hilliard equation to describe the evolution of the interface, whereas Inamuro et al. use the pressure projection method for multiphase flows with high density ratio.

The mean-field theory model proposed by He et al. (1998, 1999a) is valid in the nearly incompressible limit and applies to nonideal gases. In this model, the simulation parameters are the pressure and an index function, which is used to track the interface and plays the same role as the density difference in the free-energy model. Interfacial dynamics are modeled by introducing molecular interaction forces, which are approximated by the mean-field theory. Phase separation occurs naturally owing to the instability of the supernodal curve of the phase diagram. This model accurately simulates the Rayleigh-Taylor and Kelvin-Helmholtz instabilities, even with nonideal and dense fluids (He et al. 1999a,b). Lee & Lin (2005a) proposed a model based on the mean-field theory that can simulate two-phase flow with high density ratios. Lee & Lin's (2005a) model for high density ratio and McCracken & Abraham's (2005) MRT model for multiphase flow were combined by Mukherjee & Abraham (2007a,b), who discretized the collision term explicitly instead of semi-implicitly.

In the case of planar two-phase Poiseuille flow, the discontinuity problem at the interface has been investigated by Ginzburg (2007), who derived a two-relaxation-time (TRT) collision operator (Ginzburg 2005) to satisfy the continuity of pressure, tangential shear stress, and momentum at the interface. The TRT collision operator cannot guarantee continuity at the interface when the two fluids have different densities (Ginzburg 2007) because for the case of parabolic flow (e.g., Poiseuille flow), the pressure distribution is uniform, which means that the solution for f_i does not depend on the speed of sound or density. Therefore, the tangential velocity $u = 1/\rho \sum f_i$ is discontinuous at the interface because ρ is discontinuous. However, the TRT approach is effective for the case of a large viscosity ratio between phases.

Rannou (2008) evaluated the effectiveness of various models in maintaining the continuity of shear stress and velocity at the interface for a fully developed two-phase Poiseuille flow in a 2D channel. When the two fluids have different densities, none of the four approaches could satisfy the continuity in velocity at the interface with either the BGK or TRT collision operator. In the case of two fluids with different viscosities, the TRT approach shows great promise (see Ginzburg 2007). The free-energy model gives accurate results, except at high-viscosity ratios (>100). For low-viscosity ratios, the color-fluid model gives accurate results with either a BGK or a TRT

collision operator, but if the viscosity ratio is too high (>100), only the TRT collision operator can guarantee continuity at the interface. The interparticle-potential model leads to a discrepancy at the interface, even for low viscosity ratios. Moreover, this model is not purely immiscible, and the physical properties (viscosity and density) of the two phases do not remain constant. The mean-field theory model gives accurate results for the high-viscosity phase but poor results for the low-viscosity phase; however, no discontinuity is observed at the interface for viscosity ratios up to ∼20.

In addition to the methods outlined above, other promising methods based on a combination of the LB equation with explicit interface-tracking schemes are under development. One approach uses Peskin's (2002) distribution function for the interface force used in the immersed-boundary (IB) method (Lallemand et al. 2007). More recently, interface tracking using the level-set approach has been reported with promising results (Thömmes et al. 2009). The problem of LB simulation of the parallel flow of fluids with density variation discussed above remains open.

5. MICROFLUIDICS

Advances in nanotechnology and the use of microelectromechanical systems have spurred interest in the use of the LB method for the simulation of microfluidics (for a general review on microfluidics, see Karniadakis & Beskok 2005). In the small length scales present in these devices, the Knudsen number becomes a defining quantity. At vanishingly small Kn, the molecular mean-free path is much smaller than the characteristic length scale of the macroscopic flow. In this case, the flow can be treated as a continuum, and the NS equations apply. At the wall, the typical no-slip boundary exists.

At increasing Kn, the first notable departure from continuum behavior occurs with the creation of a slip layer at the wall at Kn ∼ 0.001, in which noncontinuum effects are limited to the near-wall region known as the Knudsen layer. In the slip regime ($0.001 < Kn < 0.1$), the Knudsen layer is small, and the bulk of the flow can be treated as a continuum fluid with a slip model accounting for the effect of the Knudsen layer. The use of the LB method is appropriate in the wall-slip regime to determine bulk flow properties. This requires implementing a slip boundary condition into the LB framework, of which two methods are proposed. The first slip-boundary method uses a combination of the no-slip bounce-back and a free-slip specular-reflection scheme (Benzi et al. 2006, Lim et al. 2002, Nie et al. 2002, Sbragaglia & Succi 2005, Succi 2002). The second method is a kinetically motivated boundary condition based on Maxwell's diffuse boundary condition for the continuous BE (Cercignani 1969), with discretized versions for the LB method given by Ansumali & Karlin (2002) and Sofonea & Sekerka (2005). These methods treat the boundary as an ideal smooth surface; however, it is also possible to generate slip behavior through surface effects (Kunert & Harting 2007, Sbragaglia et al. 2006).

As the Knudsen number increases into the transition regime ($0.1 < Kn < 10$), the Knudsen layers grow to include a large portion of the flow domain. At high enough Kn, these layers can merge, eliminating any portion of the flow in which the continuum assumption is valid. The traditional LB method is insufficient to resolve the flow characteristics within the Knudsen layer. In this layer, nonequilibrium effects create a nonlinear relationship between stress and strain. Traditional simulation approaches rely on the direct solution of the linear BE or direct simulation Monte Carlo methods. These methods are expensive computationally, particularly for low-speed flows such as those found in microfluidics.

To resolve the Knudsen layer using the LB method, two strategies exist that are typically used in conjunction with the slip boundary conditions mentioned above. The first relies on the inclusion of a wall function to alter the dynamics near the wall by adjusting the relaxation time or using a

mean-field theory approach (Guo et al. 2006; Kim et al. 2008b; Toschi & Succi 2005; Zhang et al. 2004, 2006), which is phenomenologically motivated based on the reduction in mean-free path near the wall. The other method is physically based and requires the inclusion of higher-order terms in the LB method to simulate higher-order fluid equations, such as the Burnett, super-Burnett, Grad 13-moment, or beyond. Although it is based on more detailed kinetics, historically the LB method was derived as an NS solver. As such, criticism has been raised about the validity of applying the LB method to finite-Knudsen-number flows (Guo et al. 2006, Luo 2004). This criticism stems from the classical formulation of the LB method, which is second-order accurate in the Chapman-Enskog expansion (Chen & Doolen 1998); however, the inclusion of higher-order terms is possible. Because of the cumbersome nature of the Chapman-Enskog procedure, higher-order LB methods are typically derived by projecting the BE onto a Hermite basis (Shan & He 1998). By truncating at various levels in the Hermite expansions, one can obtain differing orders of accuracy for the LB method (Chikatamarla & Karlin 2006, Shan et al. 2006); however, the roots of the higher Hermite polynomials are not rational, requiring a finite-difference scheme (Mei & Shyy 1998) or an approximation technique (Chikatamarla & Karlin 2006).

A general lack of agreement exists in the definition of Kn and λ_m in the LB literature (e.g., Guo et al. 2006, Lee & Lin 2005b, Nie et al. 2002, Toschi & Succi 2005). Care must be taken in the definition of Kn to allow comparison to existing experimental and analytical results. In general, λ_m is known exactly only for hard-sphere molecules (Chapman & Cowling 1970), and when dealing with less-well-defined intermolecular interactions, Cercignani (1988) suggests using a viscosity-based mean-free path, shown as

$$\lambda_v = \sqrt{\frac{\pi}{2}}\frac{\nu}{c_s}, \tag{25}$$

where the viscosity is related to the relaxation time τ through the BGK collision operator; consequently, many experimental and analytical results are reported with this definition. As a direct extension to the LB method, Kim et al. (2008b) suggest using the viscosity-based mean-free path, which relates the Knudsen number to the relaxation time as

$$\mathrm{Kn} = \frac{\lambda_m}{H} = \sqrt{\frac{\pi}{2}}\frac{\tau c_s}{H}. \tag{26}$$

Mixed results have been reported by investigators. Although there is increased accuracy compared with the standard LB method, results using either ELB (Ansumali et al. 2006) or higher-order D2Q13 schemes (Tang et al. 2008) fail to predict the nonlinear stress-strain relationship in the Knudsen layer without the use of a wall function. Exact solutions for planar Couette flow indicate that, given a sufficient number of velocity vectors, the LB hierarchy is capable of quantitative prediction for microflows (Ansumali et al. 2007), and renormalization techniques can be used to introduce higher-order effects into simple lattices, thus preserving computational efficiency (Karlin & Ansumali 2007). A review of several higher-order LB methods is found in Kim et al. (2008a). A particularly revealing test used by Kim et al., and shown in **Figure 2**, compares the normalized flow rate as a function of Kn for plane Poiseuille flow, in which the flow rate goes through a minimum known as the Knudsen minimum (Cercignani 1975). Several important observations are made. First, although higher-order Hermitian quadratures generally result in improved accuracy, the convergence is not monotonic. Likewise, for a given level of accuracy (**Figure 2*b***), results are highly sensitive to the chosen quadrature. For example, based on quasi-analytical results (Cercignani et al. 2004), the linearized BE shows a minimum in flow rate at Kn $\approx$ 1 and a logarithmic high-Kn asymptotic growth. In contrast, the D2Q16 and D2Q21 methods, both of seventh-order accuracy, underpredict the Knudsen minimum and show a linear high-Kn

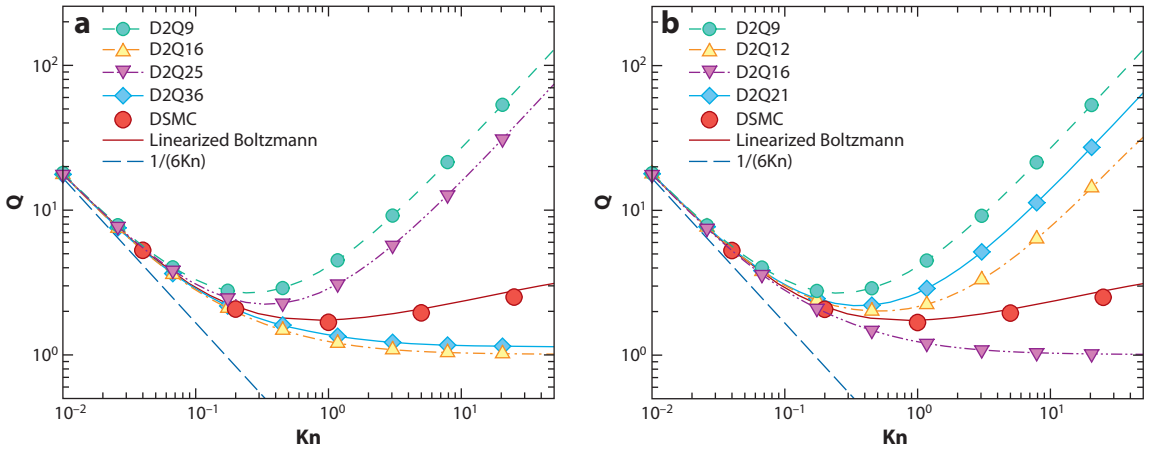

Figure 2

Normalized mass flow in plane Poiseuille flow for various lattice-Boltzmann (LB) quadratures, direct simulation Monte Carlo, and linearized Boltzmann solutions (Cercignani et al. 2004). LB results in panel *b* are seventh order, except D2Q9. Figure taken from Kim et al. 2008a.

asymptotic behavior. The D2Q16 method, also of seventh-order accuracy, does not predict a minimum in flow rate and instead converges to a constant value as Kn $\rightarrow \infty$.

Microscale flow remains an active area of research for the LB method. This method has proven to be effective when dealing with flow of moderate Kn and has some success at predicting the Knudsen layer. Resolving inconsistencies at higher Kn is paramount to the realization of the LB method as an effective microfluidic simulation alternative to the direct simulation Monte Carlo method and other computationally demanding methods.

6. PARTICLE SUSPENSIONS

6.1. Introduction

The LB method has been effective in the simulation of particle suspensions, which play an important role in many industrial and biological situations, including those as varied as paper slurries, arterial flow, and cosmetics. Even though the particles may be suspended in a Newtonian fluid, the resultant suspension exhibits much more complex and non-Newtonian flow characteristics, and understanding the complex rheology of these suspensions is important. The analytical treatment of suspensions is primarily confined to the dilute limit, where only the effect of two-body interactions is considered. The role of volume concentration on suspension viscosity was shown by Einstein (1956) for the dilute limit and extended by Batchelor & Green (1972) for two-body interactions. The extension to multibody interactions inherent in dense suspensions quickly becomes intractable analytically, except in cases involving a regular and periodic structure. A review of colloidal and noncolloidal suspension rheology can be found in Stickel & Powell (2005).

Numerical simulations are necessary to further our understanding of suspensions, and they provide a complementary investigative tool to traditional experimentation. In general, simulations can provide a more detailed description than experimentation. Also, confounding variables that can be difficult to eliminate or quantify experimentally (such as particle roughness, particle polydispersity, and interparticle forces) are easily controlled in simulations. This control allows the isolation of individual parameters for investigation. Furthermore, experimentation with fluids like blood can

create problems owing to their biological nature. Several factors explain the usefulness of the LB method in these situations. First, the LB method provides straightforward and easy-to-implement boundary conditions necessary to couple the fluid to the suspended particles. Second, the method is computationally efficient and scales linearly with the number of particles, N. The local nature and the regular lattice grid facilitate the use of the LB method on distributed-memory clusters, in contrast with competitive numerical methods such as Stokesian dynamics. Also, the dense and transient nature of suspensions limits the benefits of nonuniform grid techniques that would be commonly used in numerical schemes such as finite-element analysis (FEA). Furthermore, the LB method reproduces the full NS equations, which makes the study of inertial effects possible (Aidun et al. 1998, Ding & Aidun 2000, Qi 1999).

6.2. Rigid Particle Suspensions

Early applications of the LB method to particle suspensions include those of Ladd (1994a,b), Aidun & Lu (1995), and Aidun et al. (1998). In these early applications, the bounce-back method couples 2D cylinders, spheres, spheroids, and ellipsoids to the fluid grid, allowing moving boundaries. The SBB boundary condition (Equation 20) is still widely used, owing to its simple implementation and verified results.

The time evolution of the particle is found by solving Newton's equations of motion,

$$M\frac{d\mathbf{U}(t)}{dt} = \mathbf{F}(t) \tag{27}$$

and

$$\boldsymbol{I}\cdot\frac{\boldsymbol{\Omega}(t)}{dt} + \boldsymbol{\Omega}(t)\times[\boldsymbol{I}\cdot\boldsymbol{\Omega}(t)] = \mathbf{T}(t), \tag{28}$$

where M is the particle mass, $\boldsymbol{I}$ is the inertial tensor, $\mathbf{U}$ is the translational velocity, $\boldsymbol{\Omega}$ is the angular velocity, and $\mathbf{F}$ and $\mathbf{T}$ are the total force and torque on the particle, respectively. Ladd (1994b) demonstrated that, even with averaging over consecutive time steps, a simple central-difference explicit update is conditionally stable. This criterion puts lower bounds on the allowable mass, rotational inertia, and hence size of the suspended particles. The stability of the particle update procedure can be improved by using a higher-order integration scheme, such as a fourth-order Runge-Kutta scheme (Aidun et al. 1998), or made unconditionally stable through an implicit boundary update (Lowe et al. 1995, Nguyen & Ladd 2002). Also, the higher-order bounce-back schemes discussed in Section 6.4 improve stability.

The boundary velocity, $\mathbf{u}_b$, can be calculated as

$$\mathbf{u}_b = \mathbf{U} + \boldsymbol{\Omega}\times(\mathbf{r}_b - \mathbf{X}),$$

where $\mathbf{r}_b$ and $\mathbf{X}$ are the location of the link midpoint and particle center of mass, respectively. The resulting force and torque are calculated by summing Equation 21 over all FBNs that reside at link end points, shown as

$$\mathbf{F} = \sum_{FBN}\mathbf{F}_{i'}^{(b)}(\mathbf{x}_b, t) \quad \text{and} \quad \mathbf{T} = \sum_{FBN}(\mathbf{x}_b - \mathbf{X})\times\mathbf{F}_{i'}^{(b)}(\mathbf{x}_b, t). \tag{29}$$

The SBB operation causes mass to stream through the particle boundary, as indicated by the last term in Equation 20. This streaming of mass is necessary because the discrete velocities of $\mathbf{e}_i$ relegate the adjustment in momentum of f_i to the alteration of density. If the boundary location is set to the midpoint of the boundary link, the net mass flux for any rigid particle is zero; however, this balance can be disrupted by particles near contact (Nguyen & Ladd 2002) or deformable particles (MacMeccan et al. 2009).

Some debate has occurred over whether to include the fluid in the interior of the particle. As initially formulated by Ladd (1994a,b), particles are treated as shells of mass M containing fluid, which has the potential to affect dynamics. Ladd (1994a,b) argues the fluid will relax to rigid-body motion with a characteristic nondimensional frequency given by $\Omega^* = \Omega a^2/\nu_{\text{int}}$, where ν_{int} is the viscosity of the internal fluid. For low-frequency motion ($\Omega^* \ll 1$), the fluid relaxes completely, and the particle behaves as a rigid particle with the combined mass and moment of inertia of the shell plus the interior fluid. Thus, to simulate a particle of true neutral buoyancy in the long time limit, the mass of the shell must approach zero, which creates instabilities in the particle update procedure. For a simple explicit update, this instability can be expressed in terms of density ratio and particle size as

$$\frac{\rho_s}{\rho} > 1 + \frac{10}{a},$$

where ρ_s is the combined density of the particle shell and internal fluid (Ladd 1994b). Implicit updates have been proposed that loosen this constraint (Lowe et al. 1995). It is worth noting that the interior fluid can be assigned an arbitrarily high viscosity to ensure the relaxation to the long time limit (Ladd & Verberg 2001). In the Stokes-flow and noncolloidal limits, inertial effects are negligible, and the additional mass does not affect the dynamics.

At short times, such as those describing the Brownian motion of colloidal particles, the inertial lag of the internal fluid is appreciable and does affect particle dynamics (Heemels et al. 2000). For this reason, formulations of the LB method removing the effect of the interior fluid have been developed that capture both long and short time dynamics accurately (Aidun & Lu 1995, Aidun et al. 1998, Heemels et al. 2000). In Aidun et al.'s (1998) method, interior fluid nodes are updated as normal nodes; however, they do not contribute to particle dynamics. Thus, the summing operation in Equation 29 occurs only on exterior FBNs. In contrast, a particle containing interior fluid is implemented by summing over both interior and exterior FBNs. For nonshell particles, when fluid nodes are covered or uncovered, an additional force must be applied to the particle. This force is equivalent to the momentum difference between the solid body and newly (un)covered fluid node, and can be expressed for the case of node covering as

$$\mathbf{F}^{(c)}(\mathbf{r}, t + \tfrac{1}{2}) = \rho(\mathbf{r}, t)[\mathbf{u}(\mathbf{r}, t) - \mathbf{U}'(\mathbf{r}, t)], \tag{30}$$

where $\mathbf{U}'(\mathbf{r}, t)$ is the local velocity of the solid at the lattice node (Ding & Aidun 2003). For node uncovering, the force takes a negative sign, and a corresponding covering and uncovering torque can be calculated from the force. Including a virtual fluid mitigates the impulses applied to the particle during the covering and uncovering of fluid nodes because the fluid nodes are partially relaxed to the velocity of the boundary (Ding & Aidun 2003). The ability to simulate both solid and fluid-filled capsules remains important when the LB method is extended to deformable particles and capsules, as discussed in Section 6.5.

To simulate Brownian suspensions with the LB method, one needs to introduce stochastic fluctuations in the stress field to induce random fluctuations in particle motion. Early studies introduced a stochastic element to the collision operator, such that the fluctuations only affected the viscous stress tensor (Ladd 1994a,b). Although this reproduces correct dynamics in the hydrodynamic limit, kinetic or ghost modes of the LB equation are incorrectly thermalized, which results in errors at small length scales (Adhikari et al. 2005, Dünweg et al. 2007). A corrected scheme, referred to as the fluctuating LB equation, was proposed by Adhikari et al. (2005). Recently, analysis of the fluctuating LB equation shows a clear connection to statistical mechanics, and the fluctuating LB equation is shown to satisfy detailed balance and to correctly reproduce the fluctuation-dissipation theorem in the macroscopic regime (Dünweg et al. 2007).

Rheological quantities such as shear viscosity, normal-stress differences, and suspension pressure have been successfully calculated using the LB method (Kulkarni & Morris 2008, Lishchuk et al. 2006, MacMeccan et al. 2009). In the simplest form, shear viscosity is calculated directly via the shear stress on the simulation walls; however, at higher concentrations, depletion layers form near the wall, lowering the effective shear rate, and hence apparent viscosity, in the core. Eliminating the walls through the use of the LEbc precludes the use of wall stress in viscosity calculations. Lishchuk et al. (2006) employ a method based on relating the total dissipation to the viscosity (Einstein 1906, Landau & Lifshitz 1995). Their method accurately calculates viscosity data for a suspension in simple shear that agrees well with the empirical Krieger-Dougherty formula (Krieger & Dougherty 1959).

Another alternative is to calculate the particle stresslet, and thus the suspension stress. Following Batchelor (1970), the suspension stress can be calculated for Stokes flow by

$$\boldsymbol{\Sigma} = -P\boldsymbol{I} + 2\mu\boldsymbol{E} + \frac{1}{V}\sum \boldsymbol{S}, \tag{31}$$

where $\boldsymbol{\Sigma}$ is the volume-averaged stress in the suspension, P is the average fluid pressure, $\boldsymbol{I}$ is the identity tensor, $\boldsymbol{E}$ is the average rate of strain, $\boldsymbol{S}$ is the particle stresslet, and V is the volume of the simulation domain. The summation is over all particles in the simulation. The stresslet is calculated via a surface integral of the form

$$\boldsymbol{S} = \int_{A_0} \frac{1}{2}(\boldsymbol{\sigma}\mathbf{X} + \mathbf{X}\boldsymbol{\sigma}) \cdot \mathbf{n} - \mu(\mathbf{u}_b\mathbf{n} + \mathbf{n}\mathbf{u}_b)dA, \tag{32}$$

where $\boldsymbol{\sigma}$ is the stress in the fluid at the particle surface, and $\mathbf{n}$ is the unit vector normal to the surface. From an implementation standpoint, the first term in Equation 32 is calculated by summing over the link-wise traction vectors (see Equation 21) acting on the particle. The second term allows calculation for deformable particles, which are discussed in detail in Section 6.5. In addition to shear viscosity, the calculation of the full suspension stress tensor allows an investigation of normal stresses, which play an important role in particle migration and the development of concentration gradients (Morris & Boulay 1999, Nott & Brady 1994). Also, terms exist to extend this calculation to nonzero Reynolds numbers (Batchelor 1970), and these corrections have been successfully applied to study inertial effects in suspensions (Kulkarni & Morris 2008).

For the case of solid particles, a Galilean error exists in the standard bounce-back condition (Caiazzo & Junk 2008, Clausen & Aidun 2009). The Galilean error can be removed, in methods that are equivalent, by bouncing $f_{i'}^{e}(\rho, \mathbf{u}_b)$ from the link end point residing inside the particle (Clausen & Aidun 2009), or by subtracting the error directly (Caiazzo & Junk 2008). For fluid-filled particles, the interior nodes do affect dynamics and thus cancel the Galilean error; however, if external traction vectors are used to calculate the stresslet or other quantities, errors may still exist. The magnitude of these errors is typically small and scales as u^2. However, when computing small sensitive parameters such as normal stresses in particle suspensions, these errors may be significant.

6.3. Particles Near Contact

The LB method accurately resolves forces between particles with separations approaching one lattice unit. This accuracy corresponds to the ability of the LB method to resolve lubrication hydrodynamics as long as a single lattice node resides between two surfaces. Once particles move within one lattice spacing, however, the standard bounce-back is inadequate, and proper hydrodynamics are no longer recovered. Modeling based on lubrication theory (Cox 1974) is used to update the force and torques on two approaching particles in a pair-wise fashion.

Ladd (1997) calculates the normal forces between two spheres (denoted 1 and 2 in subscripts) according to

$$\mathbf{F}_{12} = -\frac{6\pi\mu(a_1 a_2)^2}{(a_1 + a_2)^2}\left(\frac{1}{\delta} - \frac{1}{\delta_c}\right)\mathbf{U}_{12}\cdot\hat{\mathbf{R}}_{12}\hat{\mathbf{R}}_{12},$$

where a is the radius of each respective sphere, $\hat{\mathbf{R}}_{12}$ is the unit vector connecting the particle centers, $\mathbf{U}_{12}$ is the approach velocity, δ is the gap between spheres, and δ_c is an appropriate cutoff distance to stop applying the lubrication modeling. This method is generalized by casting the interaction between particles in the grand-resistance-matrix formulation (Nguyen & Ladd 2002) using friction coefficients given by Kim & Karilla (1991). This method also accounts for tangential friction and allows the accurate calculation of the particle stresslet. Results obtained with this method compare well with analytical results (Cichocki & Jones 1998) down to particle separations of $O(0.01a)$.

An alternate lubrication correction presented by Ding & Aidun (2003) adds a link-wise correction force based on the local gap and curvature. In this case, the force applied to the solid boundary in Equation 21 is modified by adding an additional term, given by

$$df = \begin{cases} \dfrac{3\bar{q}\mu(a_1 a_2)}{2c_i^2(a_1 + a_2)}\left(\dfrac{1}{\delta^2} - \dfrac{1}{c_i^2}\right)\mathbf{U}_{12}\cdot\hat{\mathbf{R}}_{12}, & \text{if } \delta < c_i \\ 0, & \text{if } \delta \geq c_i, \end{cases}$$

where $\bar{q}$ is a weighting factor that depends on the lattice structure and is determined from simulations, and c_i^2 is a scaling factor based on the link direction. A suggested value of $\bar{q} \simeq 0.6$ gives results that compare relatively well with analytical solutions for a D3Q19 method upon summing over all links (Ding & Aidun 2003). Contact modeling can be incorporated into either model as a short-ranged repulsive force.

Nguyen & Ladd's method uses well-established methods and gives accurate results at exceedingly small gaps; however, it is restricted to simulating particles whose two-body resistance and mobility functions are known analytically. Ding & Aidun's method has the advantage of flexibility, being able to simulate arbitrarily shaped particles, but it has one important disadvantage. Namely, the lubrication model is still tied to the discrete lattice grid, which limits the minimum gap that can be resolved. Particles must be relatively larger than the lattice dimension compared with those using Nguyen & Ladd's formulation.

In addition to lubrication modeling, the standard bounce-back procedure must be modified for particles near contact. When there are no intervening fluid nodes, the use of a different velocity in the bounce-back calculation for the i and i' directions is not symmetric and does not preserve global mass or momentum (**Figure 3*a***). Ladd (1994b) suggests setting the boundary velocity, $\mathbf{u}_b$, equal to the average velocity of the two surfaces (**Figure 3*b***), which does conserve global mass and momentum. The result is an equivalent force applied to both particles that does not reproduce proper hydrodynamics, which is acceptable assuming a separate lubrication model. More importantly, a net mass flux from one particle to another occurs owing to the alteration of the boundary velocity. Although this flux is small, conservation can be ensured by tracking the change in mass on a particle-by-particle basis, and adding this extra mass to the exterior FBNs. Likewise, the force and torque on the boundary from this procedure can be updated (Nguyen & Ladd 2002). Another option treats the interior link end points as fluid nodes residing outside the particle, and the bounce-back operation is performed on the adjacent nodes (**Figure 3*c***). This scheme does capture forces when no intervening lattice nodes exist; however, the forces are inaccurate, and lubrication modeling is still necessary (Ding & Aidun 2003).

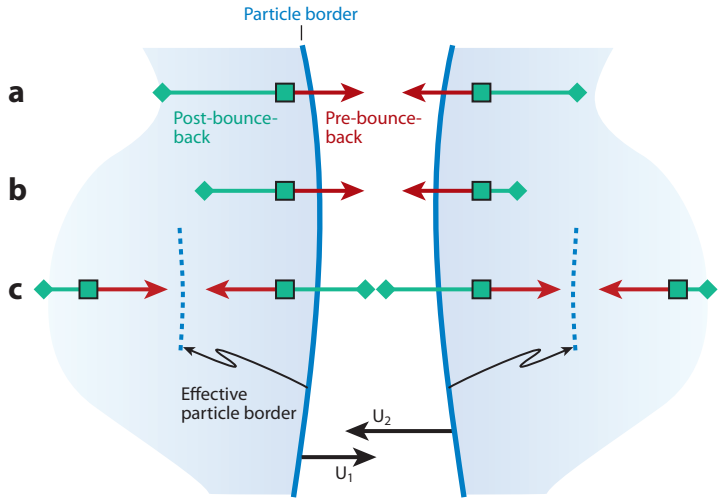

Figure 3

Two approaching particles without intervening lattice nodes, showing distributions before and after the bounce-back operation. If nodes are bounced using separate particle velocities, global mass conservation is violated (*a*), as indicated by the difference in the combined lengths of the pre- and post-bounce-back arrows. Bouncing nodes with an average velocity restores global mass conservation, but errors in force and local mass occur (*b*). Treating nodes just inside particles as fluid nodes, in effect moving the particle border (*dashed lines*), allows proper force and mass conservation (*c*).

6.4. Alternate and Higher-Order Boundary Conditions

The most widely used boundary condition for the LB method is the SBB condition for moving walls presented in Section 2.4. This method is simple to implement; however, it does have several disadvantages. First, although the method is second-order accurate when the solid boundary resides on the midpoint of the link, this is not the case for an arbitrary surface, for which the accuracy of the bounce-back method degrades into a first-order-accurate velocity field. For suspensions, the result is an error in the hydrodynamic radius of the particle. For cases of rigid particles, a priori corrections using the hydrodynamic radius through calibration simulations are possible, but not ideal (Ladd 1994b). Consequently, significant effort has gone toward improving the accuracy of the no-slip boundary conditions, and these improvements are broadly split into two groups. The first group retains its basis on links crossing the solid boundary and relies on interpolation schemes to increase the accuracy when the solid does not lie at the midpoint of the link. The second group alters fluid distributions local to the solid boundary without creating links.

6.4.1. Link-based methods. For link-based methods, the SBB method is altered to account for a boundary that does not lie at the midpoint of the link. One possible modification includes the alteration of the SBB based on the solid fraction in the Wigner-Seitz cell surrounding a lattice node (Verberg & Ladd 2001). Owing to the complexity in calculating this solid fraction, especially in three dimensions, effort has focused on interpolation methods (Filippova & Hänel 1998a, Mei et al. 2002). These methods interpolate from fluid nodes adjacent to the FBN, as depicted for linear interpolation in **Figure 4** (Bouzidi et al. 2001, Lallemand & Luo 2003). The quantity q is defined to be the boundary distance as a fraction of the total link distance, $|\mathbf{e}_i|$. For the case when the solid boundary is closer than the link midpoint, $0 < q \leq 1/2$, an interpolated distribution is created such that the bounced distribution lands on the FBN (**Figure 4*a***). For a boundary

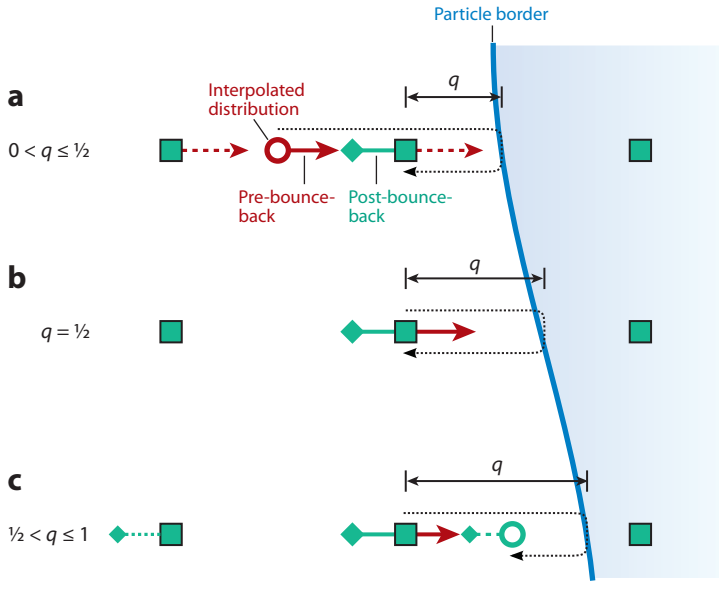

Figure 4

Linear interpolation bounce-back method showing pre- and post-bounce-back distributions. Dashed arrows represent fluid distributions used in interpolation. (*a*) The particle boundary is less than midpoint of link; thus bounce-back proceeds from an interpolated distribution (*open red circle*) calculated from neighboring distributions. (*b*) The particle boundary is at the midpoint of link, and no interpolation is required. (*c*) The particle boundary is further than the midpoint; thus the post-bounce-back distribution is bounced to an intermediate location (*open green circle*) and then interpolated to the nearest fluid boundary node with adjustment due to next-nearest fluid distribution.

at the link midpoint, $q = 0.5$, the distribution returning postbounce lands exactly on the FBN in the opposite direction (**Figure 4*b***), and no interpolation is required. For the last case, in which the solid boundary is further than the link midpoint, the distribution at the FBN is bounced to an intermediate location and then interpolated appropriately (**Figure 4*c***). Higher-order quadratic interpolation is possible (Bouzidi et al. 2001, Lallemand & Luo 2003).

With the use of the LBGK collision operator, there also exists an error in the boundary location that is dependent on the viscosity (e.g., Ding & Aidun 2003, Ladd & Verberg 2001, Noble et al. 1995). This error exists for SBB methods, even with the boundary located at the midpoint of two FBNs, and for the linear and quadratic interpolation methods mentioned above. For this reason, an MRT (d'Humières 1992) or TRT (Ginzburg 2005) collision operator is desirable because these methods allow the tuning of the free eigenvalues of the collision matrix to maintain the independence of the boundary location on the viscosity (Ginzbourg & Adler 1994, Ginzburg & d'Humières 2003).

Ginzburg & d'Humières (2003) present a general framework for analyzing and constructing these interpolation-based boundary conditions and adjusting eigenvalues for several flow conditions. For their proposed multireflection method, they directly derive the accuracies for simple cases such as Couette and Poiseuille flows and show them to be third-order accurate in the velocity field. As mentioned above, the error in the multireflection method is independent of the fluid viscosity. Numerical simulations of the multireflection boundary condition indicate an increased accuracy in more complicated geometries; however, the results show that the convergence is nonmonotonic; thus traditional analysis tools need judicious application (Bouzidi et al. 2001,

Ginzburg & d'Humières 2003). A detailed examination of interpolated-link-based methods and their convergence and viscosity dependency can be found in Pan et al. (2006).

When applied to particle suspensions, the principal disadvantage of these interpolation methods is the requirement of extra fluid nodes between particles. Junk & Yang (2005) show that attempts to use the standard bounce-back in cases in which insufficient fluid nodes exist cause errors to propagate throughout the simulation domain, thus destroying the increased accuracy of the interpolation method. In an attempt to address these shortcomings, Chun & Ladd (2007) developed a method that interpolates only the equilibrium portion of the fluid distribution. Because the nonequilibrium portion of the fluid distribution is one order of accuracy higher than the equilibrium distribution in the Chapman-Enskog expansion, combining the interpolated equilibrium and nonequilibrium distribution still results in an overall second-order accuracy. The primary advantage of this variant is the ability to prescribe an additional equilibrium distribution at the boundary surface, thus allowing the application of linear interpolation in the same situations as the original bounce-back rule. A disadvantage to all interpolation methods is the lack of mass conservation. Although the magnitude of mass leakage for the multireflection and equilibrium interpolated methods is small, it may be important in cases such as the simulation of deformable capsules, in which mass leakage results in an overall change in particle volume.

6.4.2. Node-based methods. The second group of methods increases the accuracy of the fluid-solid coupling through the direct alteration of fluid nodes adjacent to the solid surface. Although referred to as IB, early methods based on the work of Noble & Torczynski (1998) and Holdych (2003) did not have the two-grid system characteristic of traditional IB methods. Instead, these methods alter the collision operator with forcing terms dependent on the volume fraction of solid in the given lattice cell. This method requires the accurate calculation of the solid fraction for each of these cells, which is complicated for arbitrarily shaped particles in three dimensions. Without an accurate calculation of the partially filled fluid cell volume fraction, spikes in particle force and torque are reported (Strack & Cook 2007).

Feng & Michaelides (2004) take a more traditional approach to the IB method, using a Lagrangian grid to track the particle's surface in addition to the Eulerian LB method grid. The points on the Lagrangian grid are allowed to freely advect with the local fluid velocity. Then, they use a solid model to calculate a restorative force term on the Lagrangian nodes, which is typically a high-stiffness elastic model for the simulation of rigid particles. As in traditional IB techniques, the force term is applied to the fluid as a force density through an appropriate weighting function (Peskin 2002). In the LB method, this force density is prescribed through a forcing term to the LB equation (Equation 12).

In Wu & Aidun's (2009) method, the no-slip condition is enforced directly on fluid nodes adjacent to the solid in a method called the external boundary force (EBF) LB method. Similar to the IB method, EBF uses a Lagrangian mesh to track the particle. Unlike the IB method, the Lagrangian nodes are not free to advect with the local fluid velocity. Instead, a momentum deficit is calculated between the solid and fluid velocities using the same weighting functions found in the IB method. A force density necessary to impose the no-slip fluid velocity is applied to the fluid by altering the collision operator, and an equivalent momentum transfer prescribes the force on the solid.

When discussing IB and contrasting it with traditional methods, investigators often use terms such as sharp and smeared to describe the interface without adequate definition. Perhaps it is more useful to discuss how accurately each method resolves the placement of the boundary in terms of fluid-solid interactions. In all LB methods, the location of the particle boundary is known exactly in terms of either a shape function or solid Lagrangian grid; however, the fluid-solid coupling introduces an error in the location of the boundary as felt by the fluid. For example,

both the standard IB and EBF methods are formally second-order accurate (Griffith & Peskin 2005); however, at the fluid-solid boundary, these methods introduce first-order spatial errors in the velocity field, which is a by-product of the delta functions used to distribute the force density to the surrounding fluid nodes (Peskin 2002). If the definition of a smeared interface is first-order accuracy, then both the IB and EBF methods, as well as the SBB, apply. The EBF method may be extendable to second-order accuracy because the possibility exists for independently altering the momentum of fluids separated by a boundary. Although of first-order accuracy, the IB and EBF methods provide results superior to those of the SBB. In particular, the forces and torques applied to the suspended particles are much smoother than those of the SBB because the delta functions mitigate the fluctuations as lattice nodes are covered and uncovered (Feng & Michaelides 2004, Wu & Aidun 2009). Also, the IB and EBF methods provide a convenient and efficient computational tool for the simulation of deformable particle dynamics, and they eliminate the costly determination of all links crossing an arbitrarily shaped particle. Additionally, these methods do conserve global mass in the simulation domain as the force-density operation is mass conserving.

6.5. Deformable Suspensions

In some cases, treating the suspended phase as a rigid solid will not properly capture the micro- and macroscopic properties. One example that has garnered significant interest is the simulation of blood, which consists of deformable red blood cells (RBCs) suspended in plasma, a Newtonian fluid. The deformation of the suspended particles allows the particles to squeeze past one another, which results in a substantially lower viscosity than an equivalent volume fraction of rigid particles. Another example can be found in deformable-fiber suspensions, where deformation is known to cause changes in the dynamics of the fibers (Blakeney 1966, Forgacs & Mason 1959), and curved fibers can increase suspension viscosity (Joung et al. 2002). In recent years, a growing interest in these suspensions has driven the development of coupled methods, in which the LB method is combined with an appropriate solid model to capture the deformation of particles.

For deformable capsules, as in the RBC case, the relevant nondimensional parameter describing the relative effect of elastic and viscous stresses is the capillary number, defined as $Ca = \mu\dot{\gamma}a/G_m$ for an elastic membrane, where G_m is the membrane shear modulus. As the local shear increases, so does the deformation of the particle, which results in a decreased suspension viscosity. This effect causes the shear-thinning behavior of blood. Dupin et al. (2007) combine the LB method with a Lagrangian particle mesh, where constants are defined to provide resistance to shear, bending, changes in surface area, and changes in volume. Coupling to the LB-method grid is accomplished through an IB method. By using a relatively coarse mesh of approximately 400 nodes on the particle, these authors demonstrated results capturing a blunted velocity profile in a suspension of approximately 200 RBCs at 30% volume fraction.

Another method of simulating deformable capsules combines the LB method with linear-elastic finite-element modeling (MacMeccan et al. 2009). In this method, the solid particle is described by a triangular shell mesh, and the FEA equation is integrated using Newmark's method. Coupling between the LB method and FEA mesh occurs through the SBB boundary condition. This LB-FEA hybrid method is capable of simulating $O(10^2)$ particles at high volume fraction (40%) on a desktop workstation. Application of the Lees-Edwards boundary conditions (see Section 2.4) allows the calculation of bulk rheology parameters. Results of RBCs in shear show relative viscosity for a range of concentrations and capillary numbers and compare well with experimental results. A snapshot from a wall-bounded shear simulation of 2472 RBCs at 40% volume fraction is shown in **Figure 5**. Owing to the flexibility of the FEA modeling, this solid model is also appropriate for solid particles (tetrahedral elements) or even deformable fibers (beam elements). However, the

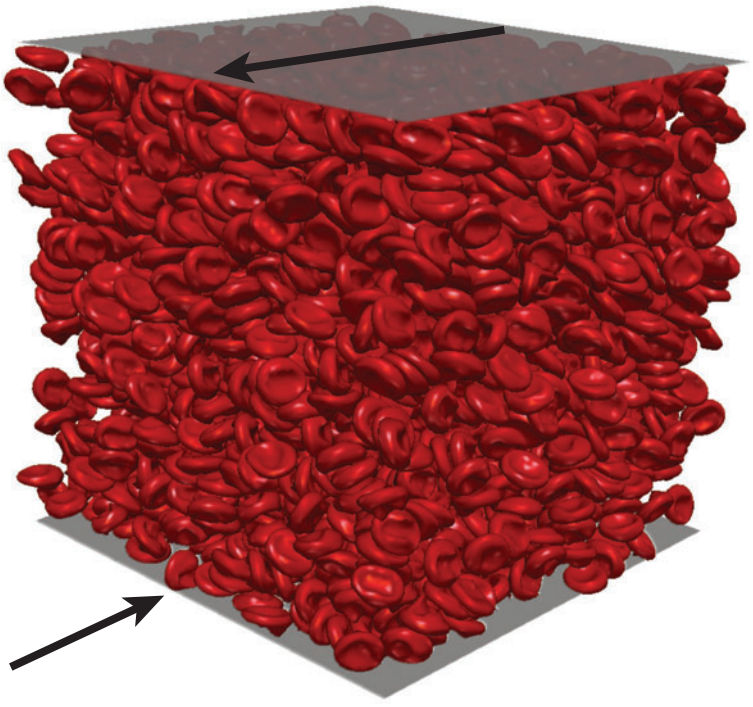

Figure 5

Wall-bounded simulation of 2472 deformable red blood cells in shear at 40% concentration. Computations by C. Aidun & J. Clausen for this article.

SBB fluid-solid coupling method is not ideal for resolving the narrow thickness of fibers, in which an IB or EBF coupling would be more appropriate.

To demonstrate the potential of the EBF approach for the simulation of deformable particles, Wu & Aidun (2009) couple the EBF method with the lattice-spring method to capture deformation of the suspended particles. Model RBCs are shown flowing through small capillaries. These RBCs deform into a parachute-like shape, and the relative deformation compares well with experimental results. Results also include the calculation of shear viscosity for 130 model RBCs at 47% volume fraction, showing good agreement with experimental results. Also, Buxton et al. (2005) use the lattice-spring method to simulate a deformable capsule impacting a wall, with the SBB coupling the lattice-spring solid to the LB fluid. Although computationally efficient for the simulation of solid particles or fibers, the lattice-spring method lacks efficiency when simulating capsules because the membrane's thickness must be resolved by several solid nodes. Additionally, Poisson's ratio, although adjustable, is dictated by the lattice-spring formulation (e.g., see Buxton et al. 2001).

The EBF method of coupling fluid to solid is not limited to rigid or lattice-spring particles. Wu & Aidun (2010) couple the LB fluid to a flexible fiber based on interconnected cylindrical sections (Lindstrom & Uesaka 2008, Schmid et al. 2000) using the EBF boundary condition. Fiber suspensions have also been simulated by Qi (2007), in which the fiber was modeled as a series of interconnected spheroids and coupled to a LB-method fluid using the SBB. In the future, incorporating the EBF boundary condition with the FEA solid model would likely combine the flexibility and efficiency of the FEA method with the increased boundary resolution and performance of the EBF method.

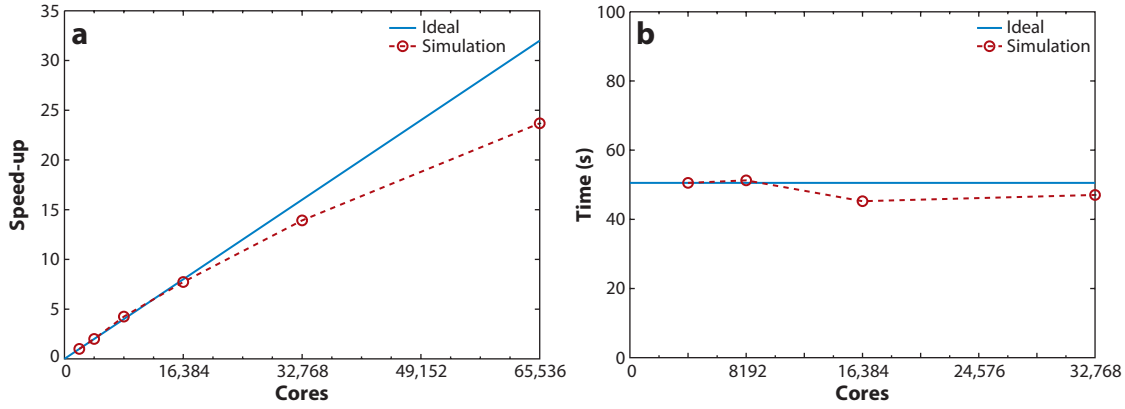

Figure 6

Scaling for single-phase lattice-Boltzmann (LB) code on BlueGene/P installation at Argonne National Lab (Clausen et al. 2009). (*a*) Strong scaling showing speed-up for 1024^3 domain in wall-bounded shear; per-core domains vary from $128 \times 64 \times 64$ to $32 \times 32 \times 16$. (*b*) Weak scaling showing time to solution of 1000 LB time steps for fixed per core domain size of $32 \times 32 \times 32$; total simulation size varies from 512^3 to 1024^3.

6.6. Parallel Implementation

Some of the most attractive features of the LB method are the ease of parallel implementation and highly scalable parallel performance. Owing to the local nature of the streaming and collisions steps, a single layer of ghost nodes is typically sufficient for decomposing the domain for distributed computational clusters. Two common methods of measuring the scaling performance exist: weak scaling and strong scaling. In weak scaling, the domain size is increased in proportion to the number of nodes or processing cores; thus the subdomain size calculated by individual cores remains fixed. The time to solution should remain constant for ideal weak scaling. Conversely, in strong scaling, the domain size is fixed while the number of processing cores is increased; thus the subdomain sizes decrease. Strong scaling results are typically presented in terms of speed-up, i.e., simulation time for a reference number of computational nodes divided by the time for an increased number of computational nodes. Ideal strong scaling is a linear increase with the slope of unity. Doubling the number of computational cores results in a speed-up of two, or half the simulation time. We have benchmarked the weak and strong scaling of the single-relaxation-time LB method on the BlueGene/P system at Argonne National Lab (Clausen et al. 2009), with scaling results up to 65,536 processor cores, as shown in **Figure 6**. This impressive scalability mirrors other researchers' results. For example, Vahala et al. (2008) reported near-perfect weak scaling for a magnetohydrodynamics LB code with a maximum of 9.1 thousand floating point operations per second (TFLOPS) on a BlueGene system using 32,764 processor cores. They also reported near-perfect weak scaling on the Earth Simulator with a maximum of 13.5 TFLOPS on 4096 processor cores. Bernaschi et al. (2009) obtained strong scaling results, showing 93% of ideal speed-up with 16,384 cores and 76% of ideal speed-up with 32,768 tasks using a molecular dynamics/LB coupled method on the BlueGene/L architecture.

Excellent scalability is seen for single-phase flow; however, the inclusion of finite-element particles complicates the parallelization. For the multiphase results shown in **Figure 7** (Clausen et al. 2009), the solid-phase finite-element calculations become a significant portion of the computational time. Thus, as the per-core domain size decreases, differences in the number of particles per core create load-balancing issues. The scalability of the suspension simulations can be improved with further optimization and better load balancing.

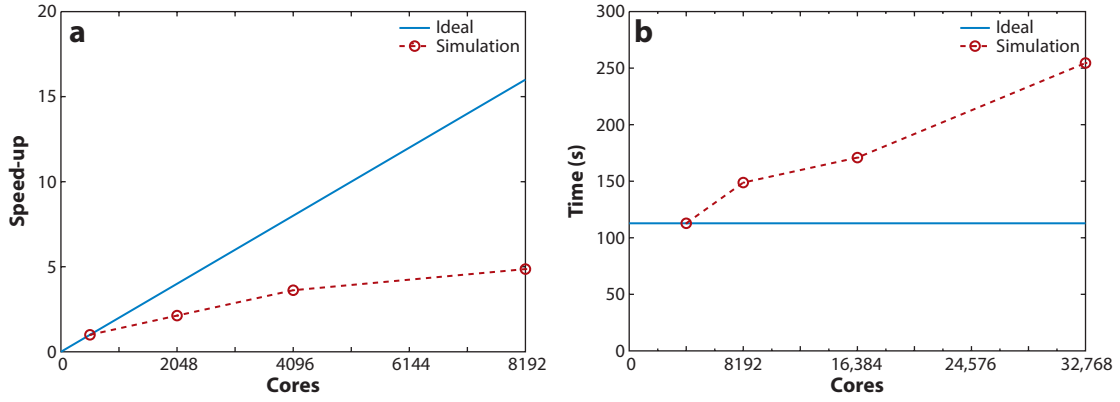

Figure 7

Scaling for multiphase lattice-Boltzmann (LB) code on BlueGene/P installation at Argonne National Lab (Clausen et al. 2009). (*a*) Strong scaling showing speed-up for 512^3 domain with 13,824 deformable particles at 40% volume fraction. (*b*) Weak scaling showing time to solution of 100 LB time steps for fixed per-core domain size of $32 \times 32 \times 32$.

7. CONCLUSIONS

The LB method has matured as a viable and efficient substitute for NS solvers in many flow problems. Particularly during the past decade, this method has found applications in complex flows, multiphase flow, micro- and nanofluidics, and turbulence, providing a new approach to these problems. The extreme simplicity of the LB equations and the local nature of the streaming-collision operations, in combination with parallel processing hardware, provide a powerful tool for analysis of flows spanning multiple scales (Succi 2008). Given the connection to the original BE with Maxwellian distribution, the LB method may be perceived as having the same limitations. This is, of course, not the case, as the local Maxwellian equilibria apply to dense as well as dilute gases, and the LB collision mean-free path in the multiple-speed collision operation can be adjusted as a free parameter to set the rate of diffusion.

The use of the LB method to probe flows in nano- and microfluidic devices has been an area of intense research in recent years. Despite early misgivings about treating the LB method as anything more than an NS solver, the underlying kinetic nature of the LB equation has proven instrumental in its application to these flows. The development of accurate, physically based kinetic boundary conditions and the extension to higher-order lattices have allowed the study of flows in the slip and transition regimes. Additionally, the LB method is vastly more computationally efficient compared with traditional simulation methods for high-Knudsen-number flows. Still, more work is needed to improve the accuracy of the LB method for microflows, particularly when the Knudsen number approaches $O(1)$, while maintaining computational efficiency.

Results have consistently shown the LB method to be a reliable, robust, and efficient method to probe the dynamics and rheology of suspensions. The BGK collision operator combined with the SBB boundary condition is the most common scheme chosen owing to its simplicity and proven results. Many alternative and higher-order boundary conditions have been developed, notably the interpolated bounce-back and immersed-boundary-type methods (IB and EBF). The interpolated bounce-back methods are undoubtedly the most accurate; however, implementation can be difficult, especially in suspensions in which particles routinely approach within a lattice spacing, and insufficient lattice sites exist to perform the required interpolations. Also, the lack of

strict mass conservation is an issue with some interpolation methods. The IB and EBF methods are easy to implement and are especially appealing when simulating arbitrarily shaped or deformable particles, in which a Lagrangian solid mesh is already prescribed.

When one extends the LB method to more complicated suspensions, resolving particle interaction in the near-contact region is still an issue. Current lubrication and contact models are too restrictive, with the two commonly used models imposing limitations. Either the shape of the particle is limited to those in which the analytical pair-wise interaction is known, which precludes the simulation of deformable particles, or the lubrication model is unnecessarily tied to the fluid mesh resolution, which limits the accuracy gains and increased fluid grid spacing realized by the higher-order boundary methods. These limitations to lubrication modeling are not unique to the LB method. Considering the large magnitude of forces that develop when particles approach one another, and the large impact these forces have on the rheology, a lubrication model that is general enough to apply to deformable particles yet independent of the underlying fluid resolution is highly desirable.

Because of space limitations, several applications of the LB method are not thoroughly covered here. For example, the LB method has been combined with molecular dynamics to simulate polymer flows as proposed by Ahlrichs & Dünweg (1998, 1999) and more recently by a number of other investigators (Malevanets & Yeomans 2000, Song et al. 2008, Xu et al. 2005). A recent review article on the subject by Dünweg (2007) indicates that as far as simulation of polymer solution is concerned, "[mesoscopic approaches] are all very similar both in terms of philosophy and (probably) computational efficiency."

Another challenging area is the application of the LB method to study reactive flows, such as isothermal reaction diffusion with no heat release (Dawson et al. 1993), 2D methane laminar flame with instantaneous chemistry and significant heat release (Succi et al. 1997), and low-Mach-number laminar combustion (Filippova & Hänel 1998b). In particular, the low-Reynolds-number flows with heterogeneous surface reaction (catalytic conversion) are well suited to reactive LB schemes (Succi et al. 1997). More recently, Yamamoto et al. (2002) proposed an LB-method-based model to simulate incompressible turbulent combustion. This model assumes that the chemical reaction does not affect the flow field, so all fields are decoupled and solved separately. The authors successfully extended their model to compressible turbulent combustion (Yamamoto 2003) and combustion in porous media (Yamamoto et al. 2004, Yamamoto & Takada 2006). The reactive LB scheme proposed by Filippova & Hänel (1998b) (low-Mach-number approximation introduced into the LB method to simulate combustion) was recently used to build a more stable model that could handle a higher temperature ratio (Chen et al. 2008).

The LB method provides an efficient approach for the solution of a large class of flow problems and a new angle of attack for the analysis of complex flows. Ideas developed over several decades for the NS equations are being rapidly incorporated into the LB method. Examples span from LES in turbulent flow to ideas from the level-set approach, IB method, and various other boundary-interaction methods in complex flows. We are excited about the continued development of the LB method, and its growing popularity among researchers for simulating an increasingly diverse array of physical problems.

DISCLOSURE STATEMENT

The authors are not aware of any affiliations, memberships, funding, or financial holdings that might be perceived as affecting the objectivity of this review.

ACKNOWLEDGMENTS

We wish to thank our colleagues I. Ginsburg, M. Junk, P. Neitzel, S. Succi, and G. Vahala for their review of this manuscript and excellent comments. The valuable comments from our colleague T. Ladd over the years are also much appreciated. The collaborations with talented scientists and colleagues Y. Lu, D. Qi, and E.J. Ding over the years are much valued. The significant contributions from R. MacMeccan to the LB-FEM are recognized. We also thank the present LB group of students in C.K.A.'s group at Georgia Tech, I. Khan, G. Rannou, D. Reasor, A. Salahuddin, J. Wu, and M. Yun who have contributed by reading and commenting on this article. The financial support to C.K.A. over the years from the National Science Foundation, the Department of Energy, and the member companies of the IPST@GT is acknowledged. Resources of the Argonne Leadership Computing Facility at Argonne National Laboratory, which is supported by the Office of Science of the U.S. Department of Energy under contract DE-AC02-06CH11357, have been used for parallel implementation.

LITERATURE CITED

Adhikari R, Stratford K, Cates ME, Wagner AJ. 2005. Fluctuating lattice Boltzmann. *Europhys. Lett.* 71:473–79

Ahlrichs P, Dünweg B. 1998. Lattice-Boltzmann simulation of polymer-solvent systems. *Int. J. Mod. Phys. C* 9:1429–38

Ahlrichs P, Dünweg B. 1999. Simulation of a single polymer chain in solution by combining lattice Boltzmann and molecular dynamics. *J. Chem. Phys.* 111:8225–39

Aidun CK, Lu Y. 1995. Lattice Boltzmann simulation of solid particles suspended in fluid. *J. Stat. Phys.* 81:49–61

Aidun CK, Lu Y, Ding EJ. 1998. Direct analysis of particulate suspensions with inertia using the discrete Boltzmann equation. *J. Fluid Mech.* 373:287–311

Ansumali S, Karlin IV. 2000. Stabilization of the lattice Boltzmann method by the H theorem: a numerical test. *Phys. Rev. E* 62:7999–8003

Ansumali S, Karlin IV. 2002. Kinetic boundary conditions in the lattice Boltzmann method. *Phys. Rev. E* 66:026311

Ansumali S, Karlin IV, Arcidiacono S, Abbas A, Prasianakis NI. 2007. Hydrodynamics beyond Navier-Stokes: exact solution to the lattice Boltzmann hierarchy. *Phys. Rev. Lett.* 98:124502

Ansumali S, Karlin IV, Frouzakis C, Boulouchos K. 2006. Entropic lattice Boltzmann method for microflows. *Phys. A* 359:289–305

Ansumali S, Karlin IV, Ottinger HC. 2003. Minimal entropic kinetic models for hydrodynamics. *Europhys. Lett.* 63:798–804

Ansumali S, Karlin IV, Succi S. 2004. Kinetic theory of turbulence modeling: smallness parameter, scaling and microscopic derivation of Smagorinsky model. *Phys. A* 338:379–94

Axner L, Latt J, Hoekstra AG, Chopard B, Sloot PMA. 2007. Simulating time harmonic flows with the regularized L-BGK method. *Int. J. Mod. Phys. C* 18:661–66

Batchelor GK. 1970. The stress system in a suspension of force-free particles. *J. Fluid Mech.* 41:545–70

Batchelor GK, Green JT. 1972. The determination of the bulk stress in a suspension of spherical particles to order c^2. *J. Fluid Mech.* 56:401–27

Benzi R, Biferale L, Sbragaglia M, Succi S, Toschi F. 2006. Mesoscopic modelling of heterogeneous boundary conditions for microchannel flows. *J. Fluid Mech.* 548:257–80

Benzi R, Succi S. 1990. Two-dimensional turbulence with the lattice Boltzmann equation. *J. Phys. A* 23:L1–5

Benzi R, Succi S, Vergassola M. 1992. The lattice Boltzmann equation: theory and applications. *Phys. Rep.* 222:145–97

Bernaschi M, Melchionna S, Succi S, Fyta M, Kaxiras E, Sircar J. 2009. Muphy: a parallel multi-physics/scale code for high performance bio-fluidic simulations. *Comput. Phys. Commun.* 180:1495–502

Blakeney WR. 1966. The viscosity of suspension of straight, rigid rods. *J. Colloid Interface Sci.* 22:324

Boghosian BM, Love P, Yepez J. 2004a. Entropic lattice Boltzmann model for Burgers's equation. *Philos. Trans. R. Soc. London Ser. A* 362:1691–701

Boghosian BM, Love PJ, Coveney PV, Karlin IV, Succi S, Yepez J. 2003. Galilean-invariant lattice-Boltzmann models with H theorem. *Phys. Rev. E* 68:025103

Boghosian BM, Love PJ, Yepez J, Coveney PV. 2004b. Galilean-invariant multi-speed entropic lattice Boltzmann models. *Phys. D* 193:169–81

Boghosian BM, Yepez J, Coveney PV, Wager A. 2001. Entropic lattice Boltzmann methods. *Proc. R. Soc. Lond. Ser. A* 457:717–66

Boltzmann L. 1872. Weitere Studien über das Wärmegleichgewicht unter Gasmolekülen. *Wien. Ber.* 66:275–370

Bonilla LL, Soler JS. 2001. High-field limit of the Vlasov-Poisson-Fokker-Planck system: a comparison of different perturbation methods. *Math. Models Methods Appl. Sci.* 11:1457–68

Bouchut F, Golse F, Pulvirenti M. 2000. *Kinetic Equations and Asymptotic Theory*. Ser. Appl. Math. No. 4. Paris: Gauthier-Villars

Bouzidi M, Firdaouss M, Lallemand P. 2001. Momentum transfer of a Boltzmann-lattice fluid with boundaries. *Phys. Fluids* 13:3452–59

Buxton G, Verberg R, Jasnow D, Balazs A. 2005. Newtonian fluid meets an elastic solid: coupling lattice-Boltzmann and lattice-spring models. *Phys. Rev. E* 71:056707

Buxton GA, Care CM, Cleaver DJ. 2001. A lattice spring model of heterogeneous materials with plasticity. *Model. Simul. Mater. Sci.* 9:485–97

Caiazzo A, Junk M. 2008. Boundary forces in lattice Boltzmann: analysis of momentum exchange algorithm. *Comput. Math. Appl.* 55:1415–23

Cercignani C. 1969. *Mathematical Methods in Kinetic Theory*. New York: Plenum

Cercignani C. 1975. *Theory and Application of the Boltzmann Equation*. New York: Elsevier

Cercignani C. 1988. *The Boltzmann Equation and Its Applications*. New York: Springer-Verlag

Cercignani C, Lampis M, Lorenzani S. 2004. Variational approach to gas flows in microchannels. *Phys. Fluids* 16:3426–37

Chapman S. 1916. On the law of distribution of molecular velocities, and on the theory of viscosity and thermal conduction, in a non-uniform simple monatomic gas. *Philos. Trans. R. Soc. London* 216:279–348

Chapman S, Cowling T. 1970. *The Mathematical Theory of Non-Uniform Gases*. Cambridge, UK: Cambridge Univ. Press

Chen H, Chen S, Matthaeus WH. 1992. Recovery of the Navier-Stokes equations using a lattice-gas Boltzmann method. *Phys. Rev. A* 45:R5339–42

Chen H, Kandasamy S, Orszag SA, Shock R, Succi S, Yakhot V. 2003. Extended Boltzmann kinetic equation for turbulent flows. *Science* 301:633–36

Chen H, Orszag SA, Staroselsky I, Succi S. 2004. Expanded analogy between Boltzmann kinetic theory of fluids and turbulence. *J. Fluid Mech.* 519:301–14

Chen S, Doolen GD. 1998. Lattice Boltzmann method for fluid flows. *Annu. Rev. Fluid Mech.* 30:329–64

Chen S, Liu Z, Tian Z, Shi B, Zheng C. 2008. A simple lattice Boltzmann scheme for combustion simulation. *Comput. Math. Appl.* 55:1424–32

Chibbaro S, Falcucci G, Chiatti G, Chen H, Shan X, Succi S. 2008. Lattice Boltzmann models for nonideal fluids with arrested phase-separation. *Phys. Rev. E* 77:036705

Chikatamarla SS, Karlin IV. 2006. Entropy and Galilean invariance of lattice Boltzmann theories. *Phys. Rev. Lett.* 97:190601

Chin J, Boek ES, Coveney PV. 2002. Lattice Boltzmann simulation of the flow of binary immiscible fluids with different viscosities using the Shan-Chen microscopic interaction model. *Philos. Trans. R. Soc. A* 360:547–58

Chun B, Ladd AJC. 2007. Interpolated boundary condition for lattice Boltzmann simulations of flows in narrow gaps. *Phys. Rev. E* 75:066705

Cichocki B, Jones R. 1998. Image representation of a spherical particle near a hard wall. *Phys. A* 258:273–302

Clausen JR, Aidun CK. 2009. Galilean invariance in the lattice-Boltzmann method and its effect on the calculation of rheological properties in suspensions. *Int. J. Multiphase Flow* 35:307–11

Clausen JR, Reasor DA, Aidun CK. 2009. Parallel performance of a lattice-Boltzmann/finite element cellular blood flow solver on the IBM Blue Gene/P architecture. *Comput. Phys. Commun.* Manuscript submitted
Cornubert R, d'Humières D, Levermore D. 1991. A Knudsen layer theory for lattice gases. *Phys. D* 47:241–259
Cox RG. 1974. The motion of suspended particles almost in contact. *Int. J. Multiphase Flow* 1:343–71
Darrozes J. 1969. Approximate solutions of the Boltzmann equation for flows past bodies of moderate curvature. In *Rarefied Gas Dynamics*, ed. L Trilling, HY Wachman, vol. 1, pp. 111–20. New York: Academic
Dawson SP, Chen S, Doolen GD. 1993. Lattice Boltzmann computations for reaction-diffusion equations. *J. Chem. Phys.* 98:1514–23
d'Humières D. 1992. Generalized lattice Boltzmann equations. In *Rarefied Gas Dynamics: Theory and Simulations*, ed. B Shizgal, D Weaver, vol. 159, pp. 450–58. Washington, DC: Am. Inst. Aeronaut. Astronaut.
d'Humières D, Bouzidi M, Lallemand P. 2001. Thirteen-velocity three-dimensional lattice Boltzmann model. *Phys. Rev. E* 63:066702
d'Humières D, Ginzburg I, Krafczyk M, Lallemand P, Luo LS. 2002. Multiple-relaxation-time lattice Boltzmann models in three dimensions. *Philos. Trans. R. Soc. London A* 360:437–51
Ding EJ, Aidun CK. 2000. The dynamics and scaling law for particles suspended in shear flow with inertia. *J. Fluid Mech.* 423:317–44
Ding EJ, Aidun CK. 2003. Extension of the lattice-Boltzmann method for direct simulation of suspended particles near contact. *J. Stat. Phys.* 112:685–708
Dong YH, Sagaut P. 2008. A study of time correlations in lattice Boltzmann-based large-eddy simulation of isotropic turbulence. *Phys. Fluids* 20:035105
Dünweg B. 2007. Computer simulations of the dynamics of polymer solutions. *J. Comput. Aid. Mater. Des.* 14:259–64
Dünweg B, Schiller UD, Ladd AJC. 2007. Statistical mechanics of the fluctuating lattice Boltzmann equation. *Phys. Rev. E* 76:036704
Dupin MM, Halliday I, Care CM, Alboul L, Munn LL. 2007. Modeling the flow of dense suspensions of deformable particles in three dimensions. *Phys. Rev. E* 75:066707
Eggels JGM. 1996. Direct and large-eddy simulation of turbulent fluid flow using the lattice-Boltzmann scheme. *Int. J. Heat Fluid Flow* 17:307–23
Einstein A. 1906. Zur theorie der brownschen bewegung. *Ann. Phys. (Leipzig)* 19:371–81
Einstein A. 1956. *Investigations on the Theory of the Brownian Movement*. New York: Dover
Enskog D. 1917. *Kinetische Theorie der Vorgäenge in mäessig verdüennten G*. Ph.D. thesis, Uppsala, Sweden
Falcucci G, Bella G, Chiatti G, Chibbaro S, Sbragaglia M, Succi S. 2007. Lattice Boltzmann models with mid-range interactions. *Commun. Comput. Phys.* 2:1071–84
Feng ZG, Michaelides EE. 2004. The immersed boundary-lattice Boltzmann method for solving fluid-particles interaction problems. *J. Comput. Phys.* 195:602–28
Filippova O, Hänel D. 1998a. Boundary-fitting and local grid refinement for lattice-BGK models. *Int. J. Mod. Phys. C* 9:1271–79
Filippova O, Hänel D. 1998b. Lattice-BGK model for low Mach number combustion. *Int. J. Mod. Phys. C* 9:1439–45
Forgacs OL, Mason SG. 1959. Particle motions in sheared suspensions. IX. Spin and deformation of threadlike particles. *J. Colloid Interface Sci.* 14:457–72
Frisch U, d'Humières D, Hasslacher B, Lallemand P, Pomeau Y, Rivet JP. 1987. Lattice gas hydrodynamics in two and three dimensions. *Complex Syst.* 1:649–707
Gell-Mann M, Tsallis C, eds. 2004. *Nonextensive Entropy*. Oxford: Oxford Univ. Press
Ginzbourg I, Adler P. 1994. Boundary flow condition analysis for the three-dimensional lattice Boltzmann model. *J. Phys. II* 4:191–214
Ginzbourg I, Adler PM. 1995. Surface-tension models with different viscosities. *Transport Porous Media* 20:37–76
Ginzburg I. 2005. Equilibrium-type and link-type lattice Boltzmann models for generic advection and anisotropic-dispersion equation. *Adv. Water Resour.* 28:1171–95
Ginzburg I. 2007. Lattice Boltzmann modeling with discontinuous collision components: hydrodynamic and advection-diffusion equations. *J. Stat. Phys.* 126:157–206

Ginzburg I, d'Humières D. 2003. Multireflection boundary conditions for lattice Boltzmann models. *Phys. Rev. E* 68:066614

Ginzburg I, Steiner K. 2002. A free-surface lattice Boltzmann method for modelling the filling of expanding cavities by Bingham fluids. *Philos. Trans. R. Soc. A* 360:453–66

Giraud L, D'Humieres D, Lallemand P. 1998. A lattice Boltzmann model for Jeffreys viscoelastic fluid. *Europhys. Lett.* 42:625–30

Grad H. 1958. Principles of the kinetic theory of gases. *Handb. Phys.* 12:205–51

Grad H. 1963. Asymptotic theory of the Boltzmann equation. *Phys. Fluids* 6:147–81

Griffith BE, Peskin CS. 2005. On the order of accuracy of the immersed boundary method: higher order convergence rates for sufficiently smooth problems. *J. Comput. Phys.* 208:75–105

Grunau DW, Chen S, Eggert K. 1993. A lattice Boltzmann model for multiphase fluid flows. *Phys. Fluids A* 5:2557–62

Gunstensen AK, Rothman DH, Zaleski S, Zanetti G. 1991. Lattice Boltzmann model of immiscible fluids. *Phys. Rev. A* 43:4320–27

Guo Z, Zhao TS, Shi Y. 2006. Physical symmetry, spatial accuracy, and relaxation time of the lattice Boltzmann equation for microgas flows. *J. Appl. Phys.* 99:074903

He X, Chen S, Doolen GD. 1998. A novel thermal model for the lattice Boltzmann method in incompressible limit. *J. Comput. Phys.* 146:282–300

He X, Chen S, Zhang R. 1999a. A lattice Boltzmann scheme for incompressible multiphase flow and its application in simulation of Rayleigh-Taylor instability. *J. Comput. Phys.* 152:642–63

He X, Zhang R, Chen S, Doolen GD. 1999b. On the three-dimensional Rayleigh-Taylor instability. *Phys. Fluids* 11:1143–52

Heemels MW, Hagen MHJ, Lowe CP. 2000. Simulating solid colloidal particles using the lattice-Boltzmann method. *J. Comput. Phys.* 164:48–61

Higuera FJ, Jimenez J. 1989. Boltzmann approach to lattice gas simulations. *Europhys. Lett.* 9:663–68

Hilbert D. 1902. Mathematical problems. *Bull. Am. Math. Soc.* 8:437–79

Hilbert D. 1912. *Grundzüge einer allgemeinen Theorie der linearen Integralgleichungen*. Leipzig: Teubner

Holdych D. 2003. *Lattice Boltzmann methods for diffuse and mobile interfaces*. Ph.D. thesis, Univ. Illinois, Urbana-Champaign

Holdych D, Rovas D, Georgiadis J, Buckius R. 1998. An improved hydrodynamics formulation for multiphase flow lattice-Boltzmann models. *Int. J. Mod. Phys. C* 9:1393–404

Hou S, Sterling J, Chen S, Doolen GD. 1996. A lattice Boltzmann subgrid model for high Reynolds number flows. *Fields Inst. Commun.* 6:151–66

Huang K. 1963. *Statistical Mechanics*. New York: Wiley

Inamuro T, Konishi N, Ogino F. 2000. A Galilean invariant model of the lattice Boltzmann method for multiphase fluid flows using free-energy approach. *Comput. Phys. Commun.* 129:32–45

Inamuro T, Ogata T, Tajima S, Konishi N. 2004. A lattice Boltzmann method for incompressible two-phase flows with large density differences. *J. Comput. Phys.* 198:628–44

Joung CG, Phan-Thien N, Fan XJ. 2002. Viscosity of curved fibers in suspension. *J. Non-Newton. Fluid* 102:1–17

Junk M, Klar A, Luo LS. 2005. Asymptotic analysis of the lattice Boltzmann equation. *J. Comput. Phys.* 210:676–704

Junk M, Yang Z. 2005. One-point boundary condition for the lattice Boltzmann method. *Phys. Rev. E* 72:066701

Junk M, Yang Z. 2009. Convergence of lattice Boltzmann methods for Navier-Stokes flows in periodic and bounded domains. *Numer. Math.* 112:65–87

Junk M, Yong W. 2003. Rigorous Navier-Stokes limit of the lattice Boltzmann equation. *Asymptot. Anal.* 35:165–85

Junk M, Yong W. 2009. Weighted L_2 stability of the lattice Boltzmann method. *SIAM J. Numer. Anal.* 47:805–27

Kalarakis AN, Burganos VN, Payatakes AC. 2002. Galilean-invariant lattice-Boltzmann simulation of liquid-vapor interface dynamics. *Phys. Rev. E* 65:056702

Kandhai D, Koponen A, Hoekstra A, Kataja M, Timonen J, Sloot PMA. 1999. Implementation aspects of 3D lattice-BGK: boundaries, accuracy, and a new fast relaxation method. *J. Comput. Phys.* 150:482–501

Kang HS, Chester S, Meneveau C. 2003. Decaying turbulence in an active-grid-generated flow and comparisons with large-eddy simulation. *J. Fluid Mech.* 480:129–60
Kang Q, Zhang D, Chen S. 2002. Displacement of a two-dimensional immiscible droplet in a channel. *Phys. Fluids* 14:3203–14
Kang Q, Zhang D, Chen S. 2004. Immiscible displacement in a channel: simulations of fingering in two dimensions. *Adv. Water Resour.* 27:13–22
Karlin IV, Ansumali S. 2007. Renormalization of the lattice Boltzmann hierarchy. *Phys. Rev. E* 76:025701
Karlin IV, Ferrante A, Ottinger HC. 1999. Perfect entropy functions of the lattice Boltzmann method. *Europhys. Lett.* 47:182–88
Karniadakis G, Beskok A. 2005. *Microflows and Nanoflows: Fundamentals and Simulation*. New York: Springer
Keating B, Vahala G, Yepez J, Soe M, Vahala L. 2007. Entropic lattice Boltzmann representations required to recover Navier-Stokes flows. *Phys. Rev. E* 75:036712
Kelvin L. 1887. Stability of fluid motion: rectilinear motion of viscous fluid between two parallel plates. *Philos. Mag* 24:188–96
Kim S, Karilla S. 1991. *Microhydrodynamics: Principles and Selected Applications*. Boston: Butterworth-Heinemann
Kim SH, Pitsch H, Boyd ID. 2008a. Accuracy of higher-order lattice Boltzmann methods for microscale flows with finite Knudsen numbers. *J. Comput. Phys.* 227:8655–71
Kim SH, Pitsch H, Boyd ID. 2008b. Slip velocity and Knudsen layer in the lattice Boltzmann method for microscale flows. *Phys. Rev. E* 77:026704
Koga T. 1970. *Introduction to Kinetic Theory*. New York: Pergamon
Krieger IM, Dougherty TJ. 1959. A mechanism for non-Newtonian flow in suspensions of rigid spheres. *J. Rheol.* 3:137–52
Kulkarni PM, Morris JF. 2008. Suspension properties at finite Reynolds number from simulated shear flow. *Phys. Fluids* 20:040602
Kunert C, Harting J. 2007. Roughness induced boundary slip in microchannel flows. *Phys. Rev. Lett.* 99:176001
Ladd AJC. 1994a. Numerical simulations of particulate suspensions via a discretized Boltzmann equation. Part 1. Theoretical foundation. *J. Fluid Mech.* 271:285–309
Ladd AJC. 1994b. Numerical simulations of particulate suspensions via a discretized Boltzmann equation. Part 2. Numerical results. *J. Fluid Mech.* 271:311–39
Ladd AJC. 1997. Sedimentation of homogeneous suspensions of non-Brownian spheres. *Phys. Fluids* 9:491–99
Ladd AJC, Verberg R. 2001. Lattice-Boltzmann simulations of particle-fluid suspensions. *J. Stat. Phys.* 104:1191–251
Lallemand P, Luo LS. 2003. Lattice Boltzmann method for moving boundaries. *J. Comput. Phys.* 184:406–21
Lallemand P, Luo LS, Peng Y. 2007. A lattice Boltzmann front-tracking method for interface dynamics with surface tension in two dimensions. *J. Comput. Phys.* 226:1367–84
Landau L, Lifshitz E. 1995. *Fluid Mechanics*. London: Butterworth-Heinemann
Latt J, Chopard B. 2006. Lattice Boltzmann method with regularized pre-collision distribution functions. *Math. Comput. Simul.* 72:165–68
Latva-Kokko M, Rothman DH. 2005. Diffusion properties of gradient-based lattice Boltzmann models of immiscible fluids. *Phys. Rev. E* 71:056702
Lee T, Lin CL. 2005a. A stable discretization of the lattice Boltzmann equation for simulation of incompressible two-phase flows at high density ratio. *J. Comput. Phys.* 206:16–47
Lee T, Lin CL. 2005b. Rarefaction and compressibility effects of the lattice-Boltzmann-equation method in a gas microchannel. *Phys. Rev. E* 71:046706
Lees AW, Edwards SF. 1972. The computer study of transport processes under extreme conditions. *J. Phys. C* 5:1921–28
Lim CY, Shu C, Niu XD, Chew YT. 2002. Application of lattice Boltzmann method to simulate microchannel flows. *Phys. Fluids* 14:2299–308
Lindstrom SB, Uesaka T. 2008. Simulation of semidilute suspensions of non-Brownian fibers in shear flow. *J. Chem. Phys.* 128:024901
Lishchuk SV, Care CM, Halliday I. 2003. Lattice Boltzmann algorithm for surface tension with greatly reduced microcurrents. *Phys. Rev. E* 67:036701

Lishchuk SV, Halliday I, Care CM. 2006. Shear viscosity of bulk suspensions at low Reynolds number with the three-dimensional lattice Boltzmann method. *Phys. Rev. E* 74:017701
Lowe CP, Frenkel D, Masters AJ. 1995. Long-time tails in angular momentum correlations. *J. Chem. Phys.* 103:1582–87
Luo LS. 2004. Comment on "Discrete Boltzmann equation for microfluidics." *Phys. Rev. Lett.* 92:139401
MacMeccan RM, Clausen JR, Neitzel GP, Aidun CK. 2009. Simulating deformable particle suspensions using a coupled lattice-Boltzmann and finite-element method. *J. Fluid Mech.* 618:13–39
Malevanets A, Yeomans J. 2000. Dynamics of short polymer chains in solution. *Europhys. Lett.* 52:231–37
Martinez D, Matthaeus WH, Chen S, Montgomery DC. 1994. Comparison of spectral method and lattice Boltzmann simulations of two-dimensional hydrodynamics. *Phys. Fluids* 6:1285–98
Maxwell JC. 1867. On the dynamical theory of gases. *Philos. Trans. R. Soc. London* 157:49–88
McCracken ME, Abraham J. 2005. Multiple-relaxation-time lattice-Boltzmann model for multiphase flow. *Phys. Rev. E* 71:036701
McNamara GR, Garcia AL, Alder BJ. 1995. Stabilization of thermal lattice Boltzmann models. *J. Stat. Phys.* 81:395–408
McNamara GR, Zanetti G. 1988. Use of the Boltzmann equation to simulate lattice-gas automata. *Phys. Rev. Lett.* 61:2332–35
Mei R, Shyy W. 1998. On the finite difference-based lattice Boltzmann method in curvilinear coordinates. *J. Comput. Phys.* 143:426–48
Mei R, Yu D, Shyy W, Luo LS. 2002. Force evaluation in the lattice Boltzmann method involving curved geometry. *Phys. Rev. E* 65:041203
Meyers J, Sagaut P. 2006. On the model coefficients for the standard and the variational multi-scale Smagorinsky model. *J. Fluid Mech.* 569:287–319
Morris JF, Boulay F. 1999. Curvilinear flows of noncolloidal suspensions: the role of normal stresses. *J. Rheol.* 43:1213–37
Mukherjee S, Abraham J. 2007a. A pressure-evolution-based multi-relaxation-time high-density-ratio two-phase lattice-Boltzmann model. *Comput. Fluids* 36:1149–58
Mukherjee S, Abraham J. 2007b. Lattice Boltzmann simulations of two-phase flow with high density ratio in axially symmetric geometry. *Phys. Rev. E* 75:026701
Nguyen NQ, Ladd AJC. 2002. Lubrication corrections for lattice-Boltzmann simulations of particle suspensions. *Phys. Rev. E* 66:046708
Nie X, Doolen GD, Chen S. 2002. Lattice-Boltzmann simulations of fluid flows in MEMS. *J. Stat. Phys.* 107:279–89
Noble DR, Chen S, Georgiadis JG, Buckius RO. 1995. A consistent hydrodynamic boundary condition for the lattice Boltzmann method. *Phys. Fluids* 7:203–9
Noble DR, Torczynski JR. 1998. A lattice-Boltzmann method for partially saturated computational cells. *Int. J. Mod. Phys. C* 9:1189–201
Nott PR, Brady JF. 1994. Pressure-driven suspension flow: simulation and theory. *J. Fluid Mech.* 275:157–99
Nourgaliev RR, Dinh TN, Theofanous TG, Joseph D. 2003. The lattice Boltzmann equation method: theoretical interpretation, numerics and implications. *Int. J. Multiphase Flow* 29:117–69
Orlandini E, Swift MR, Yeomans JM. 1995. A lattice Boltzmann model of binary-fluid mixtures. *Europhys. Lett.* 32:463–68
Pan C, Luo LS, Miller CT. 2006. An evaluation of lattice Boltzmann schemes for porous medium flow simulation. *Comput. Fluids* 35:898–909
Peskin CS. 2002. The immersed boundary method. *Acta Numer.* 11:479–517
Qi DW. 1999. Lattice-Boltzmann simulations of particles in non-zero-Reynolds-number flows. *J. Fluid Mech.* 385:41–62
Qi DW. 2007. A new method for direct simulations of flexible filament suspensions in non-zero Reynolds number flows. *Int. J. Numer. Methods Fluids* 54:103–18
Qian YH, d'Humières D, Lallemand P. 1992. Lattice BGK models for Navier-Stokes equation. *Europhys. Lett.* 17:479–84
Qian YH, Succi S, Orszag SA. 1995. Recent advances in lattice Boltzmann computing. *Annu. Rev. Comput. Phys.* 3:195–242

Qin RS. 2006. Mesoscopic interparticle potentials in the lattice Boltzmann equation for multiphase fluids. *Phys. Rev. E* 73:066703
Rannou G. 2008. *Lattice-Boltzmann method and immiscible two-phase flow*. Master's thesis. Georgia Inst. Technol.
Reis T, Phillips TN. 2007. Lattice Boltzmann model for simulating immiscible two-phase flows. *J. Phys. A* 40:4033–53
Rothman DH, Keller JM. 1988. Immiscible cellular-automaton fluids. *J. Stat. Phys.* 52:1119–27
Sbragaglia M, Benzi R, Biferale L, Succi S, Sugiyama K, Toschi F. 2007. Generalized lattice Boltzmann method with multirange pseudopotential. *Phys. Rev. E* 75:026702
Sbragaglia M, Benzi R, Biferale L, Succi S, Toschi F. 2006. Surface roughness-hydrophobicity coupling in microchannel and nanochannel flows. *Phys. Rev. Lett.* 97:204503
Sbragaglia M, Succi S. 2005. Analytical calculation of slip flow in lattice Boltzmann models with kinetic boundary conditions. *Phys. Fluids* 17:093602
Schmid CF, Switzer LH, Klingenberg DJ. 2000. Simulations of fiber flocculation: effects of fiber properties and interfiber friction. *J. Rheol.* 44:781–809
Shan X, Chen H. 1993. Lattice Boltzmann model for simulating flows with multiple phases and components. *Phys. Rev. E* 47:1815–19
Shan X, Chen H. 1994. Simulation of nonideal gases and liquid-gas phase transitions by the lattice-Boltzmann equation. *Phys. Rev. E* 49:2941–48
Shan X, Chen H. 2007. A general multiple-relaxation-time Boltzmann collision model. *Int. J. Mod. Phys. C* 18:635–43
Shan X, He X. 1998. Discretization of the velocity space in the solution of the Boltzmann equation. *Phys. Rev. Lett.* 80:65–68
Shan X, Yuan XF, Chen H. 2006. Kinetic theory representation of hydrodynamics: a way beyond the Navier-Stokes equation. *J. Fluid Mech.* 550:413–41
Smagorinsky J. 1963. General circulation experiments with the primitive equations: I. The basic experiments. *Mon. Weather Rev.* 91:99–164
Sofonea V, Sekerka RF. 2005. Boundary conditions for the upwind finite difference lattice Boltzmann model: evidence of slip velocity in micro-channel flow. *J. Comput. Phys.* 207:639–59
Sone Y. 1969a. Asymptotic theory of flow of rarefied gas over a smooth boundary I. In *Rarefied Gas Dynamics*, ed. L Trilling, HY Wachman, vol. 1, pp. 243–53. New York: Academic
Sone Y. 1969b. Asymptotic theory of flow of rarefied gas over a smooth boundary II. In *Rarefied Gas Dynamics*, ed. D Dini, vol. 2, pp. 737–49. Pisa: Ed. Tec. Sci.
Song KX, Jia YX, Sun ZY, An LJ. 2008. Lattice Boltzmann study of hydrodynamic effects in lamellar ordering process of two-dimensional quenched block copolymers. *J. Chem. Phys.* 129:144901
Stickel JJ, Powell RL. 2005. Fluid mechanics and rheology of dense suspensions. *Annu. Rev. Fluid Mech.* 37:129–49
Strack OE, Cook BK. 2007. Three-dimensional immersed boundary conditions for moving, solids in the lattice-Boltzmann method. *Int. J. Numer. Methods Fluids* 55:103–25
Succi S. 2001. *The Lattice Boltzmann Equation for Fluid Dynamics and Beyond*. Oxford: Clarendon
Succi S. 2002. Mesoscopic modeling of slip motion at fluid-solid interfaces with heterogeneous catalysis. *Phys. Rev. Lett.* 89:064502
Succi S. 2008. Lattice Boltzmann across scales: from turbulence to DNA translocation. *Eur. Phys. J. B* 64:471–79
Succi S, Bella G, Papetti F. 1997. Lattice kinetic theory for numerical combustion. *J. Sci. Comput.* 12:395–408
Sukop MC, Thorne DT Jr. 2006. *Lattice Boltzmann Modeling: An Introduction for Geoscientists and Engineers*. New York: Springer
Swift MR, Orlandini SE, Osborn WR, Yeomans JM. 1996. Lattice Boltzmann simulations of liquid-gas and binary fluid systems. *Phys. Rev. E* 54:5041–52
Tang GH, Zhang YH, Emerson DR. 2008. Lattice Boltzmann models for nonequilibrium gas flows. *Phys. Rev. E* 77:046701
Thömmes G, Becker J, Junk M, Vaikuntam AK, Kehrwald D, et al. 2009. A lattice Boltzmann method for immiscible multiphase flow simulations using the level set method. *J. Comput. Phys.* 228:1139–56

Toschi F, Succi S. 2005. Lattice Boltzmann method at finite Knudsen numbers. *Europhys. Lett.* 69:549–55
Tsallis C. 1988. Possible generalizations of Boltzmann-Gibbs statistics. *J. Stat. Phys.* 52:479–87
Vahala G, Keating B, Soe M, Yepez J, Vahala L, et al. 2008. MHD turbulence studies using lattice Boltzmann algorithms. *Commun. Comput. Phys.* 4:624–46
Vahala G, Keating B, Soe M, Yepez J, Vahala L, Ziegeler S. 2009. Entropic, LES and boundary conditions in lattice Boltzmann simulations of turbulence. *Eur. Phys. J. Spec. Top.* 171:167–71
Vahala G, Soe M, Ziegeler S, Yepez J, Vahala L. 2007. *Lattice Boltzmann algorithms for fluid turbulence*. Presented at *DoD High Perform. Comput. Mod. Prog. Users Group Conf., Pittsburg*
Verberg R, Ladd AJC. 2001. Accuracy and stability of a lattice-Boltzmann model with subgrid scale boundary conditions. *Phys. Rev. E* 65:016701
Wagner AJ, Pagonabarraga I. 2002. Lees-Edwards boundary conditions for lattice Boltzmann. *J. Stat. Phys.* 107:521–37
Wagner AJ, Yeomans JM. 1999. Phase separation under shear in two-dimensional binary fluids. *Phys. Rev. E* 59:4366–73
Wolf-Gladrow DA. 2000. *Lattice-Gas Cellular Automata and Lattice Boltzmann Models: An Introduction*. New York: Springer
Wu J, Aidun CK. 2009. Simulating 3D deformable particle suspensions using lattice Boltzmann method with discrete external boundary force. *Int. J. Numer. Methods Fluids* In press; doi:10.1002/fld.2043
Wu J, Aidun CK. 2010. A method for direct simulation of flexible fiber suspensions using lattice-Boltzmann equation with external boundary force field. *J. Multiphase Flow.* In press; doi: 10.1016/j.ijmultiphaseflow.2009.11.003
Xu A, Gonnella G, Lamura A, Amati G, Massaioli F. 2005. Scaling and hydrodynamic effects in lamellar ordering. *Europhys. Lett.* 71:651–57
Yamamoto K. 2003. LB simulation on combustion with turbulence. *Int. J. Mod. Phys. C* 17:197–200
Yamamoto K, He X, Doolen GD. 2002. Simulation of combustion field with lattice Boltzmann method. *J. Stat. Phys.* 107:367–83
Yamamoto K, He X, Doolen GD. 2004. Combustion simulation using the lattice Boltzmann method. *JSME Int. J. B* 47:403–9
Yamamoto K, Takada N. 2006. LB simulation on soot combustion in porous media. *Phys. A* 362:111–17
Yuan P, Schaefer L. 2006. Equations of state in a lattice Boltzmann model. *Phys. Fluids* 18:042101
Zhang J, Li B, Kwok DY. 2004. Mean-field free-energy approach to the lattice Boltzmann method for liquid-vapor and solid-fluid interfaces. *Phys. Rev. E* 69:032602
Zhang R, He X, Doolen GD, Chen S. 2001. Surface tension effects on two-dimensional two-phase Kelvin-Helmholtz instabilities. *Adv. Water Resour.* 24:461–78
Zhang YH, Gu XJ, Barber RW, Emerson DR. 2006. Capturing Knudsen layer phenomena using a lattice Boltzmann model. *Phys. Rev. E* 74:046704
Zheng HW, Shu C, Chew YT. 2006. A lattice Boltzmann model for multiphase flows with large density ratio. *J. Comput. Phys.* 218:353–71
Zhou J. 2004. *Lattice Boltzmann Methods for Shallow Water Flows*. New York: Springer
Ziegler DP. 1993. Boundary conditions for lattice Boltzmann simulations. *J. Stat. Phys.* 71:1171–77

Annual Review of
Fluid Mechanics

Volume 42, 2010

Contents

Indexes

Errata

An online log of corrections to *Annual Review of Fluid Mechanics* articles may be found at http://fluid.annualreviews.org/errata.shtml